CHALMERS
UNIVERSITY OF TECHNOLOGY

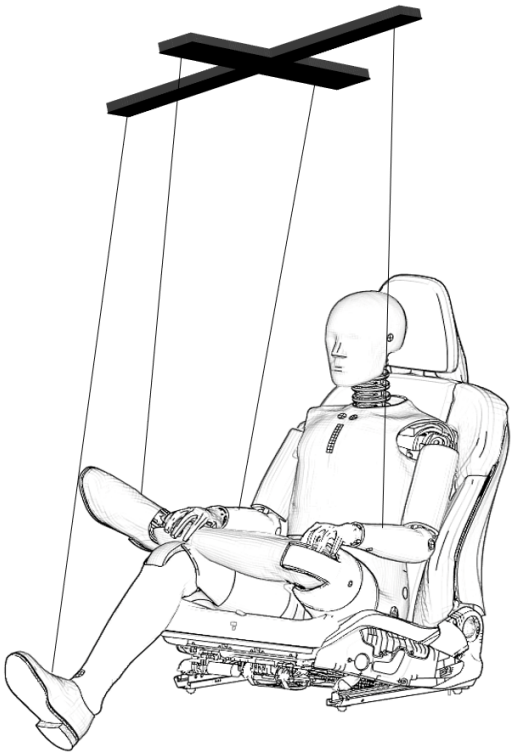

Automation of ATD positioning for crash analysis simulation

Master's thesis in Mobility Engineering

KHASHAYAR ASADI
KRISTOFFER KARLSSON

DEPARTMENT OF MENCHANICS AND MARITIME SCIENCES

CHALMERS UNIVERSITY OF TECHNOLOGY
Gothenburg, Sweden 2023
www.chalmers.se

MASTER'S THESIS IN MOBILITY ENGINEERING

Automation of ATD positioning for crash analysis simulation

KHASHYAR ASADI, KRISTOFFER KARLSSON

Department of Mechanics and Maritime Sciences
Division of Vehicle Safety
CHALMERS UNIVERSITY OF TECHNOLOGY
Göteborg, Sweden 2023

Automation of ATD positioning for crash analysis simulation
KHASHYAR ASADI, KRISTOFFER KARLSSON

Master's Thesis
Department of Mechanics and Maritime Sciences
Division of Vehicle Safety
Chalmers University of Technology

SE-412 96 Göteborg

Sweden

Telephone: + 46 (0)31-772 1000

Cover:
Anthropomorphic Test Device positioned in a car seat, attached to strings to look like a marionette puppet as a reference to manipulation of the ATD position. Furthermore, it is also a reference to the 'Marionette method' later mentioned in this report.

Chalmers Reproservice
Göteborg, Sweden 2023-06-27

Automation of ATD positioning for crash analysis simulation
Master's thesis in Mobility Engineering
KHASHYAR ASADI, KRISTOFFER KARLSSON

Department of Mechanics and Maritime Sciences
Division of Vehicle Safety

Chalmers University of Technology

Abstract

In alignment with the United Nations target 11.2, regulators enforce minimum safety requirements in different new car markets, at the same time consumer information organizations and car manufacturers strive to make cars safer. Standardized test procedures using anthropomorphic test devices (ATD) are commonly used to evaluate car crashworthiness and occupant protection. Using computer aided engineering (CAE) utilizing finite element (FE) analysis, standardized test procedures can be reconstructed in simulations. Although, safety development using CAE can be complex given the variations found in standardized test procedures in different new car markets.

This study developed an automated positioning method using intersection checks and node-to-node distance minimization for ATDs in CAE. The method was developed for the Hybrid III adult ATDs for frontal crash evaluation and was implemented for use at the car manufacturer using the simulation pre-processor ANSA's application programming interface. Three ATDs were considered and were positioned automatically in car environment models. To evaluate the methods positioning performance, an automatically positioned 50th percentile Hybrid III male model was compared with physical positioning. The driver's position in US NCAP full frontal rigid barrier 35 mph was used. The automatically positioned Anthropomorphic Test Device was positioned within two standard deviations of physical positioning for both X- and Z- coordinates in five out of six measurement locations.

Furthermore, two application studies were performed using sled simulations and a mid-size SUV developed at the car manufacturer. The studies were again assessed using the Hybrid III 50th percentile male and the US NCAP Full Frontal Rigid Barrier. The first study assessed global injury criteria reproducibility as results can vary due to model decomposition, i.e., numerical noise. In the environment and load case studied, global injury criteria showed a Coefficient of Variation regarding reproducibility of 0,65% to 4,22%. The second study assessed global injury criteria sensitivity to variations in hip-positioning. The hip-positions were retrieved from physical positioning. In this study, chest deflections showed variations up to 3.5 mm and femur force variations up to one kN for hip-positions within two standard deviations of data in physical Anthropomorphic Test Device positioning. Generally, injury criteria were more sensitive to H-point variations then model decomposition. These results stress the importance of achieving the correct H-point position, in CAE and in physical crash tests.

Keywords: Hybrid III, ATD, dummy, H-point, positioning, CAE

Preface

This master's thesis, exploring the opportunities regarding automatic Anthropomorphic Test Device positioning in Computer Aided Engineering, was conducted at Volvo Cars Safety Centre in collaboration with the frontal crash occupant interior team. The thesis was conducted from January 2023 to June 2023.

Acknowledgement

We would like to mediate our utmost appreciation for the warm welcome we have received from the team as well as the guidance we have received from our supervisor at Volvo Cars, **Gustav Bergh** and co-supervisor, **Arturo Pérez**. In addition, we want to thank our examiner **Johan Iraeus** at Chalmers University of Technology.

We would like to thank **Jonas Östh** for the guidance to sources and regarding writing as well as **Peter Appelgren** for the support on ANSA's application programming interface when it was needed the most. We would also like to thank **David Beskow** for helping us with the trickiest of LS-DYNA issues.

During the thesis we have participated in two courses. Thanks to **Jonas Bergman** and **Tina Mayberry** for arranging and letting us participate in the academic writing course. Furthermore, we would like to thank **DYNAmore Nordic**, **Anders Bernhardsson** and **Marcus Gustavsson** for providing the course Introduction to LS-DYNA.

Not to be forgotten are the master thesis colleagues, **Ali Riazi**, **Emma Djerf**, **Niklas Holländer,** and **Ellen Ryckenberg**, that have given our time in the Safety Centre library a silver lining.

Göteborg June 2023-06-27

KHASHYAR ASADI, KRISTOFFER KARLSSON

Contents

Preface III
Acknowledgement III
Contents IV
List of Figures VI
List of Tables IX
Notations X
Abbreviations XI
1 Introduction 1
1.1 Aim 2
1.2 Limitations 3
2 Background 4
2.1 Anthropomorphic Test Devices 4
2.2 Injury criteria 6
2.3 Basics of crash modelling in CAE 8
2.4 Basics of ATD positioning in CAE 8
2.5 Numerical reproducability 9
3 Method 10
3.1 Development of ATD positioning method 11
3.1.1 General automated positioning techniques 12
3.1.2 General for all seating positions 13
3.1.3 First row seating positions 13
3.1.4 Driver feet 15
3.1.5 Passenger feet 16
3.1.6 Driver hands 17
3.1.7 Passenger arm and hands 18
3.1.8 General for second row seating positions 18
3.1.9 Performance validation of positioning method 19
3.1 Application studies: Injury Criteria variation 20
3.1.1 Model decomposition 21
3.1.2 H-point positioning 22
4 Result 23
4.1 Automated ATD Positioning 23
4.1.1 Model prerequisites 23
4.1.2 Implementation 24

4.1.3 Positioning Hybrid III fifth percentile female 24
4.1.4 Positioning Hybrid III 50th percentile male 27
4.1.5 Positioning Hybrid III 95th percentile male 29
4.1.6 Performance validation 31
4.2 Application studies: Injury Criteria variation 37
4.2.1 Model decomposition 38
4.2.2 H-point movement 40
5 Discussion 44
5.1 Physical ATD positioning data 44
5.2 Automated positioning method 44
5.3 Application studies: Injury criteria variation 46
5.3.1 Injury criteria variations due to model decomposition 47
5.3.2 Injury criterion variations due to H-point movement 47
6 Conclusion 48
7 Future Work 49
8 References 50

List of Figures

Figure 1: Hybrid III 50th percentile male head instrumentation board. 5
Figure 2: Hybrid III chest displacement transducer. 6
Figure 3: Illustration of H-point and R-point. 8
Figure 4: Illustration of car seat in the car coordinate system. 10
Figure 5: Simplified flowchart of the implementation of the automated positioning method. 11
Figure 6: Exaggerated intersection between ATD foot and surface. 12
Figure 7: Illustration of Centre-to-Centre (CC) and Outer-to-Outer (OO) distance. 13
Figure 8: Upper leg rotation around hip-joint horizontal axis 14
Figure 9: Lower leg rotation around knee joint 14
Figure 10: Leg rotation outwards.....15
Figure 11: Rotating foot, centre of ball to centre of foot stand.....15
Figure 12: Foot rotated to rest on foot stand. 16
Figure 13: Downward and upward foot rotation. 16
Figure 14: Outward rotation of the foot. 16
Figure 15: Upper arm angle movement......17
Figure 16: Yoke angle, elbow angle, lower arm angle, respectively......17
Figure 17: Adjust yoke angle to backrest 18
Figure 18: Initial squatting position in second row 19
Figure 19: Demonstration of measuring nodes for validation of ATD positioning. ...20
*Figure 20: Illustration of model decomposition using *CONTROL_MPP_DECOMPOSITION_TRANSFORMATION with the flag SX and 160 CPU cores.*.....21
Figure 21: Scatter plot of H-point positions measured in physical tests, represented with black dots. 22
Figure 22: Illustration of nose-to-belt distance......22
Figure 23: Graphical User Interface.....24
Figure 24: Hybrid III fifth percentile positioned in driver seating position according to the EU NCAP protocol. 25
Figure 25: fifth percentile Hybrid III female positioned in passenger seat. 26
Figure 26: fifth percentile Hybrid III female in left, second row seating position......26

Figure 27: Hybrid III 50th percentile positioned in driver seat according to the US NCAP protocol. 27
Figure 28: Hybrid III 50th percentile male positioned in passenger seat according to the EU NCAP frontal impact procedure. 28
Figure 29: Hybrid III 50th percentile positioned in second row right seating position. 28
Figure 30: Hybrid III 95th percentile male positioned in driver seat. 29
Figure 31: Hybrid III 95th percentile male positioned in passenger seat. 30
Figure 32: Hybrid III 95th percentile male positioned in the left-hand-side second row seating position. 30
Figure 33: CAE and Physical measurements of 50th percentile Hybrid III in driver's position. 31
Figure 34: H-point X- and Z-coordinate from physical testing compared to CAE. Red, dashed vertical is the physical test mean and the dashed and dotted black line the CAE position. 32
Figure 35: Scatter plot of the physical H-point positions, shown in black, compared to the CAE estimation, shown in red. 32
Figure 36: Head X- and Z-coordinate variation from physical testing compared to CAE. Red, dashed vertical is the physical test mean and the dashed and dotted black line the CAE position. 33
Figure 37: Scatter plot of ATD head position from physical positioning data, in black, compared to the automatically positioned ATD, in red. 33
Figure 38: Nose X- and Z-coordinate variation from physical testing compared to CAE. Red, dashed vertical is the physical test mean and the dashed and dotted black line the CAE position. 34
Figure 39: Scatter plot of ATD nose position from physical positioning data, in black, compared to the automatically positioned ATD, in red. 34
Figure 40: Shoulder X- and Z-coordinate variation from physical testing compared to CAE. Red, dashed vertical is the physical test mean and the dashed and dotted black line the CAE position. 35
Figure 41: Scatter plot of shoulder coordinates from physical positioning, shown in black, compared to the automatically positioned ATD, shown in red. 35

Figure 42: Knee X- and Z-coordinate variation from physical testing compared to CAE. Red, dashed vertical is the physical test mean and the dashed and dotted black line the CAE position. 36
Figure 43: Heel X- and Z-coordinate from physical testing compared to CAE. Red, dashed vertical is the physical test mean and the dashed and dotted black line the CAE position. 36
Figure 44: Scatter plot of heel positions from physical positioning, shown in black, compared to the automatically positioned ATD, shown in red. 37

List of Tables

Table 1: Available ATDs and corresponding load type for automotive restraint system evaluation (Schmitt, 2009). 4
Table 2: Summary of results from study on injury criteria variation due to model decomposition. 38
Table 3: Normalized HIC15 as result of changes in CPU core count. 38
Table 4: Normalized NIJ as result of changes in CPU core count. 38
Table 5: Normalized neck upper force as result of changes in CPU core count. 39
Table 6: Normalized chest deflection as result of changes in CPU core count. 39
Table 7: Normalized left femur force as result of changes in CPU core count. 39
Table 8: Normalized right femur force as result of changes in CPU core count. 40
Table 9: Normalized HIC15 as result of H-point variation. 40
Table 10: Normalized Nij as result of H-point variation. 41
Table 11: Normalized neck upper force as result of H-point variation. 41
Table 12: Normalized chest deflection as function of H-point variation. 41
Table 13: Normalized nose-to-belt distance. 42
Table 14: Normalized left femur force as function of H-point variation. 42
Table 15: Normalized right femur force as function of H-point variation. 43

Notations

F_z	Axial force measured by the upper neck load cell.
F_{zc}	Critical value of the axial force measured by the upper neck load cell.
M_y	Bending moment at the occipital condyle.
M_{ocy}	Bending moment at the occipital condyle.
M_{yc}	Critical value of bending moment at the occipital condyle.
a_r	Resultant head acceleration.
μ	Average
σ	Standard deviation

Abbreviations

ATD	Anthropomorphic Test Device
API	Application Programming Interface
CAE	Computer Aided Engineering
CC	Centre-to-Centre
CD	Chest Deflection
CoG	Centre of Gravity
CPU	Central Processing Unit
CV	Coefficient of Variation
FE	Finite Element
FEM	Finite Element Method
GUI	Graphical User Interface
HBM	Human Body Model
HIC	Head Injury Criterion
HPC	High Performance Computer
MBS	Multi Body System
MPI	Message Parsing Interface
NCAP	New Car Assessment Program
NHTSA	National Highway Traffic Safety Administration
N_{ij}	Neck Injury Criterion
NUF	Neck Upper Force
OO	Outer-to-Outer

1 Introduction

In the United Nations Agenda 2030 goals, making cities and communities safe is one of the targets within the 11th goal of sustainable development: supplying access to safe transport by improving road safety (United Nations, 2023). At the same time, approximately 1.3 million people pass away each year because of road traffic crashes (World Health Organization, 2022). In alignment with the United Nations goal, regulators decide upon and enforce the absolute minimum safety standards on their governing markets. Furthermore, safety features and cars safety performances can be hard to obtain and by its nature, might be hard to interpret by someone not educated within the field. Therefore, consumer test organizations, e.g., the New Car Assessment Programs (NCAP), help and inform prospective car buyers, on the car market. By providing factual safety information to consumers, the aim is to encourage car manufacturers to introduce evidence-based safety designs beyond legislative norms (European Commision, 2023). Although, some car manufacturers have much higher ambitions and go the extra mile to develop the safest cars; not just according to consumer information test protocols but based on commonly occurring real world crashes (Jakobsson et al., 2014), backed by real world data, comprising of statistical data and in-depth crash data (Jakobsson et al., 2016).

Physical crash tests according to standardized test procedures, have for many years been the industry standard for comparing crashworthiness. Crashworthiness refers to a vehicles ability to protect occupants during a collision (Díaz & Costas, 2020). In 1970 the National Highway Traffic Safety Administration was established in the United States of America (USA). Eight years later they launched the first consumer information program, assessing occupant safety using a standardized test procedure, describing a 35-mph frontal crash test (NHTSA, 2023), using Anthropomorphic Test Devices (ATD) (Keegan, 2023).

ATDs, commonly called crash test dummies, are well defined test objects used in crash safety tests to measure the kinetics and kinematics that a human would endure in different crash scenarios (Schmitt, 2009). There exists a range of different ATDs, which come in different sizes, often referred to by percentile and sex (Nice, 2023). The Hybrid III adult ATDs comes in three sizes, representing a fifth percentile female, 50^{th} percentile male and 95^{th} percentile male.

However, performing physical crash tests is both time consuming and capital intensive, which is why Computer Aided Engineering (CAE) is utilized by car manufacturers as a complement to physical crash tests. In CAE, finite element (FE) models and Multiphysics software, like LS-DYNA (ANSYS/LST, Livermore, CA), are utilized to simulate crash scenarios: e.g., ATD models placed into car models to simulate a response for a given load case.

Car markets around the world have different legal and consumer protocols for crash safety tests (Schmitt, 2009). Variations between these protocols result in an extensive range of different positioning setups for the different ATD models. ATD positioning in CAE for every individual test protocol can be time-consuming, as it is a meticulous work performed manually. Furthermore, quality and repeatability might be subject to personal variability when different engineers are performing the procedure. Although, even if human errors during the pre-simulation setup and ATD positioning in CAE are removed, uncertainties and assumptions in modelling may hamper accuracy (Skotny,

2023). In addition, the results from simulation will inevitably be influenced by background noise and round-off effects. A study found that occupant crash simulation responses can vary due to model decomposition depending on changes in computer hardware and software (Östh et al., 2021).

For FE crash simulations, model decomposition is the process of dividing the model into smaller pieces for simulation purposes, which enables simulations to distribute workload between central processing units (CPU) and CPU cores. It is necessary to split the workload since vehicle safety FE simulations are too large to efficiently be solved using one CPU. Numerical repeatability (Östh et al., 2021), defined as using the same computer hardware and software setup, should produce the same result every time. Numerical reproducibility (Östh et al., 2021), defined as running the same simulation on different hardware and software can, theoretically, result in different simulation results (Diethelm, 2011). With increasing domains of car safety development and testing moving to CAE, knowledge about repeatability and reproducibility play an influential role in taking accurate development decisions.

Studies have investigated the repeatability and reproducibility of physical ATDs before. Among other, (Kim et al., 2017) demonstrated repeatable responses for the THOR-LX lower limbs under axial loads up to ten kN as well as (Foster et al., 1977) who showed that the Hybrid III ATD had a repeatability Coefficient of Variations (CV) of approximately five percent in physical tests. Issues regarding repeatability and reproducibility of physical ATDs is due to manufacturing tolerances, variations in positioning, and environmental conditions like temperature. However, the effects of numerical roundoff on numerical repeatability and reproducibility are largely unknown and unrecognized by CAE engineers. Although, perfect repeatability and reproducibility can be achieved (Diethelm, 2011).

1.1 Aim

The aim of this master's thesis was to develop an automated ATD positioning method for CAE that eliminates user inconsistency and increase the efficiency of the process in comparison to the current, manual, positioning method. Furthermore, the aim was to validate the automatic positioning method by comparing the final ATD position to measurements from physical ATD positioning. The expected outcome was a validated and efficient automated ATD positioning method for use in simulation modelling.

The automated positioning method was used to conduct two application studies. The first study aimed to quantify injury criteria reproducibility in car crash simulations using ATD models due to model decomposition. The second study aimed to quantify injury criteria variations due to the natural spread of hip-positioning found in physical testing.

1.2 Limitations

The development of the automated positioning method did not aim to address every available ATD and seating position but covered a majority of the most common frontal impact adult ATDs in commonly occurring regulatory and consumer rating test protocols. Furthermore, the development of the automated positioning method and its associated implementation was limited to using functions available within the programming language and the pre-processor API. Due to time limitations, protocol exceptions to ATD positioning were not considered.

As for the application studies assessing injury criteria variation due to model decomposition and ATD positioning in CAE. The studies only investigated the effects of differences in core count and hip-positioning variations found in physical test data at the car company. Comparing injury criteria variations due to variations in e.g., ATD head, thorax, and limb positioning was disregarded. To limit the use of cluster time and due to accessibility of hip positioning data, only one load case, the US NCAP Full Frontal Rigid Barrier 35 mph, and Hybrid III 50th percentile male, positioned in the driver's seat was considered.

2 Background

Regulators, consumer test organizations, and car developers, all use standardized test procedures to validate a cars safety with respect to their requirements. Due to there being more than 15 different consumer test organizations (CARHS, 2023) in addition to regulators, in different regions, with different aims and requirements, numerous different test procedures are implemented around the globe to assess vehicle safety (Schmitt, 2009). The vast number of different test procedures and requirements become very apparent for a car developer that sells cars in different markets across the globe (Schmitt, 2009).

This chapter covers some of the basics of ATDs and injury criteria as well as an introduction to crash modelling, ATD positioning and some of the uncertainties related to crash simulations.

2.1 Anthropomorphic Test Devices

ATDs are commonly employed in standardized test procedures to reproduce the loads that a human would be exposed to during a crash (Schmitt, 2009). There are a range of ATDs, for different load cases as well as a range of sizes based on anthropometric data. The construction of an ATD should be based upon anthropometry and have certain degree of bio-fidelity. That is, constructed in a way such that its joints, size, mass distribution, moments of inertia as well as posture should represent a human and have a human-like biomechanical response (Schmitt, 2009). The construction governing the biomechanical response can differ depending on which load case and injury mechanism the ATD was designed to examine. Injury mechanism refers to the type of trauma caused by its associated forces and how they impact the human body (Toney-Butler & Varacallo, 2023),

There are more than twenty different ATD types currently used in automotive crash testing developed for different load cases and in diverse sizes to model different anthropometric body sizes (Schmitt, 2009). *Table 1* demonstrates the variety of available ATDs and corresponding load cases.

Table 1: Available ATDs and corresponding load type for automotive restraint system evaluation (Schmitt, 2009).

LOAD TYPE	ANTROPOMORCHIC TEST DEVICES
FRONTAL	Hybrid III, THOR
LATERAL	EuroSID, EuroSID2, SID, SID-HIII, SID IIs, BioSID, WorldSID
REAR-END	BioRID, RID2

The Hybrid III family of adult ATDs consists of fifth percentile female, 50th male, and 95th male. The 50th percentile version of the Hybrid III ATD is the most widely used ATD for frontal impact load cases (Humanetics Innovative Solutions, Inc, 2023), regulated by US Code of Federal Regulations (2023) and referenced by European ECE Regulations. The Hybrid III family has a skull made of cast aluminimum, vinyl skin and a neck consisting of aluminum and rubber bushings held together by a cable. The head and neck construction allows to accurately simulate the flexion and extension response during high loading of the head and neck (Schmitt, 2009). The ribs are constructed of steel damped by a polymer material, attached at the thoracic spine. The pelvis consist of a casted aluminium pelvis bone moulded into urethane foam,

attaching the femurs using ball joints with integrated bump stops. The knee is constructed to evaluate ligament injury (Schmitt, 2009).

It is crucial to accurately capture the impact dynamics to examine the injury mechanisms (Schmitt, 2009). Therefore, the instrumentation does need to be sensitive and durable enough to capture the parameters associated with the injury mechanisms and associated with the load case. To capture the impact dynamics of the Hybrid III ATDs, they are equipped with sensors such as accelerometers, load cells and displacement transducers (Humanetics Innovative Solutions, Inc, 2023). The sensors mentioned in this thesis are the accelerometer located at the head Centre of Gravity (CoG), the load cell located in the upper neck, the thorax displacement transducer as well as the load cells located within the femurs of the ATD.

Figure 1 below show the head instrumentation location for the 50th percentile Hybrid III male. The accelerometer is located on the head instrumentation board at the head CoG. Also shown in *Figure 1*, is the upper neck load cell, connecting the head to the neck with a revolute joint. The upper neck load cell is capable of measuring both axial force as well as bending moments.

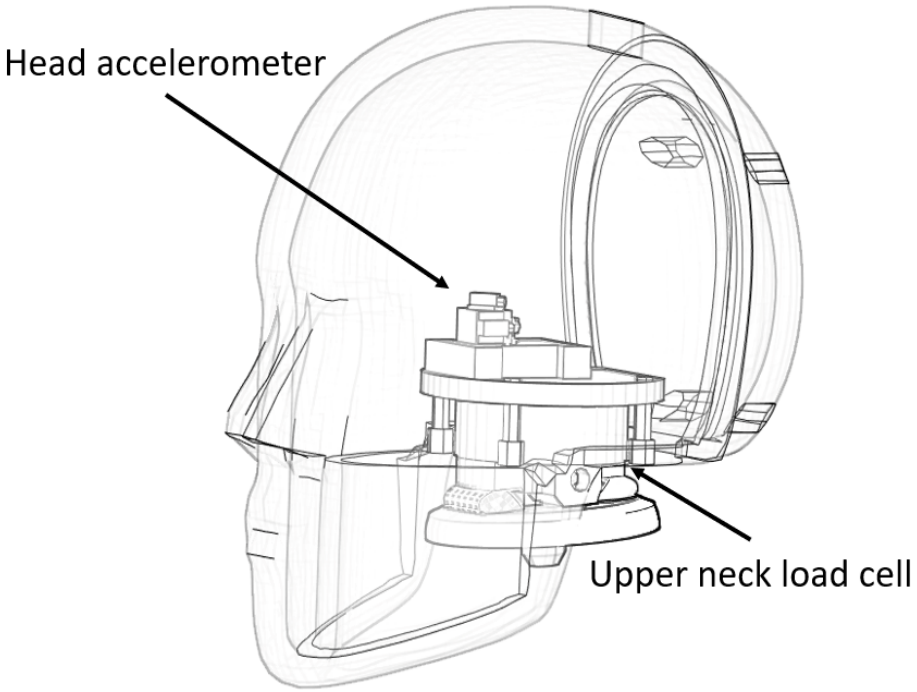

Figure 1: Hybrid III 50th percentile male head instrumentation board.

The thorax displacement transducer, shown in *Figure 2*, is positioned at the sternum of the Hybrid III ATDs. A rotational potentiometer is mounted at the thoracic spine, connected by a lever to a slider mechanism located at the sternum. When the chest is compressed relative to the spine, a ball connected to the lever runs up or down the slider mechanism changing the output of the potentiometer (Rouhana, 1998). In addition to being unreliable this way of measuring chest deflection is sensitive to how the shoulder belt is routed (Haight et al., 2013).

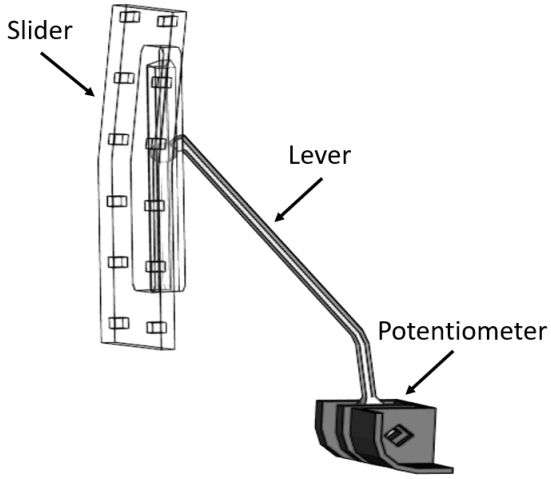

Figure 2: Hybrid III chest displacement transducer.

The femur load cells, one in each femur, are incorporated axially in the lower part of the femurs connecting the femur to the kneecap. The load cells are capable of measuring bending moments as well as axial force.

Regarding durability, the ATD shall not break during tests and be possible to repair if it does, which is why in ATD design, the construction must obtain the requirements on repeatability and reproducibility. In physical crash testing, the definition of repeatability is performing the same test repeatedly using the same ATD. For instance, (Foster et al., 1977) showed that the Hybrid III had a repeatability CV of five percent. The term reproducibility refers to the ability to compare test results obtained under identical test conditions (Schmitt, 2009).

In CAE ATDs are represented using highly detailed and validated FE models to accurately represent their physical counterparts (Altair, 2023). ATD FE models are delivered for a variety of popular FE solvers and in some instances with tunable parameters to capture variations in reproducibility between physical ATDs of the same model (Humanetics Innovative Solutions, Inc, 2023).

2.2 Injury criteria

From an engineering point of view, injury criteria can be used to evaluate the risk of injury during an impact (Germanetti et al., 2022). For ATDs, injury criteria are commonly based upon kinematics, displacements and forces measured by the ATDs sensors (Insurance Institute for Highway Safety, 2023). In this section, the injury criteria included within US NCAP full frontal rigid barrier protocol (CARHS, 2023), later mentioned in this report, are described.

Head injury criterion:
Head Injury Criterion (HIC) is a measurement of how likely it is for head injury in the form of skull fracture to arise as a function of head acceleration during an impact event. It is calculated according to *Equation 1* below. The resultant head acceleration, a_r, is measured at the center of gravity in the ATDs head and expressed as a multiple of the acceleration of gravity (g) (49 CFR 571.271 Revised as of Apr. 9, 2004). The

duration of the measurement, in the case of HIC_{15}, $(t_2 - t_1)$, is fifteen milliseconds where the mean resultant acceleration is the highest.

$$HIC_{15} = \left[\frac{1}{t_2 - t_1}\int_{t_1}^{t_2} a_r \, dt\right]^{2.5} (t_2 - t_1) \qquad (1)$$

Neck injury criterion:
The neck injury criterion, N_{ij}, is a relation between the forces and moments during loading of the upper neck connected to the risk of injury during an event (Johnson et al., 2020). F_z is the axial force and M_y is the bending moment measured by the ATD upper neck loadcell. F_z can be in either tension or compression. The bending moment at the occipital condyle, M_{ocy}, is calculated at the joint between the upper neck loadcell and the cervical spine. The bending moment can be in either flexion or extension, which results in a total of four different loading modes (49 CFR Part 571, Subpart B, 2023). F_{zc} and M_{yc} are critical values of axial force and bending moment, respectively. For the Hybrid III 50th percentile ATD, according to 49 CFR part 571, Subpart B, the critical values are:

$F_{zc} = 6806N$ when the axial force is in tension.
$F_{zc} = 6160N$ when the axial force is in compression.
$M_{yc} = 310Nm$ when moment at the occipital condyle is in flexion.
$M_{yc} = 135Nm$ when moment at the occipital condyle is in extension.

Equation 2 below shows the formula for calculating N_{ij}. The maximum value is obtained by the maximum value of the four different loading modes.

$$N_{ij} = \frac{F_z}{F_{zc}} + \frac{M_{ocy}}{M_{yc}} \qquad (2)$$

Neck tension/compression:
Neck axial force, F_z, is measured at the upper neck loadcell and can be in either tension or compression (49 CFR 572.33 Revised as of Apr. 9, 2004). Neck tension/compression is one of the components of N_{ij}.

Chest deflection:
Chest deflection is measured as the sternum's compressive deflection relative the spine in millimeters (49 CFR 572.36 Revised as of Apr. 9, 2004). For the Hybrid III family of ATDs, the measurement is recorded using the chest displacement transducer previously described.

Femur force:
The force transmitted axially through each of the femurs (49 CFR 572.36 Revised as of Apr. 9, 2004) measured using the loadcells located within the femur structure of the Hybrid III ATD.

2.3 Basics of crash modelling in CAE

Computer simulations play a role in reconstructing standardized test procedures and performing virtual testing to evaluate the crashworthiness of cars, as it allows car manufacturers to develop and design cars with reduced physical verification. Due to, advancement in computational power and numerical methods, simulations have become more detailed and powerful (Schmitt, 2009). FEM is a modelling technique that involves representing a continuous system as a discrete numerical model. The system gets devided into smaller elements consisting of nodes which makes up a mesh of the underlying geometry (Belytschko et al, 2014). The mesh and boundary conditions govern the degree of freedom of the system. This modelling technique is suitable for finding displacement, stresses in materials and contact interactions (Schmitt, 2009).

2.4 Basics of ATD positioning in CAE

ATDs are positioned by translation of the ATD and rotation of ATD joints, which can be changed either in steps of angles or by dragging and dropping in the graphical user interface of the simulation pre-processor. The ATD is translated into the seat so that the coordinates of the H-point, the theoretical centre of rotation between the ATDs torso and thighs, is correctly offset the coordinate of the R-point. The R-point refers to a vehicle manufacturer design coordinate for each designated seating position (UNECE, 2021). *Figure 3* illustrates the H-point and R-point locations before the ATD is translated to match the coordinates.

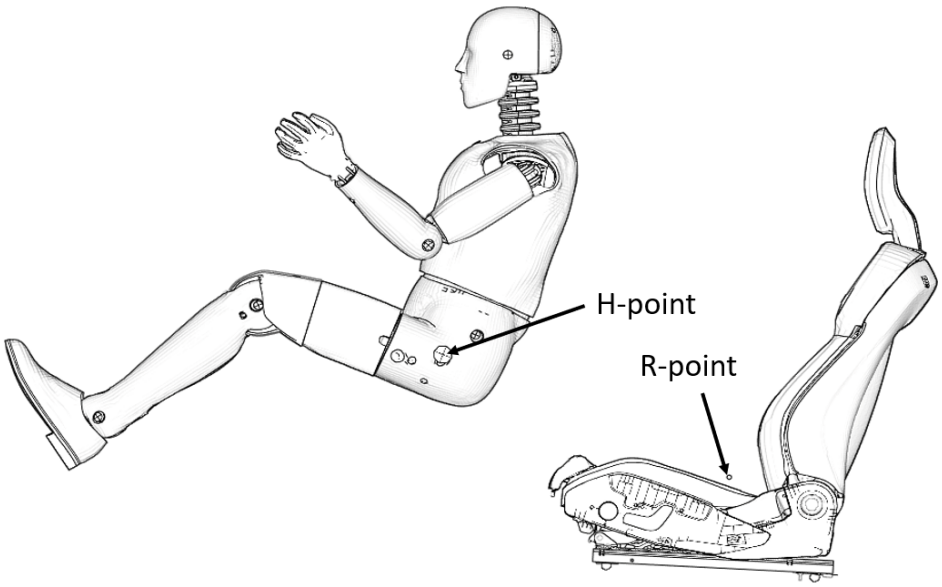

Figure 3: Illustration of H-point and R-point.

To position the ATD correctly in the seat, an H-point positioning offset should be used. The R-point in the seat is measured by a device called the H-point manikin which measures for which a ATDs H-point would be positioned in a specific seat. The H-point manikin machines theoretical H-point do not perfectly line up with the H-point of every ATD. Therefore, a H-point position offset is needed to correctly position the ATD in the seat. The pelvis is, by rotation of the hip around the H-point, positioned in the angle described in the protocol and the limbs are rotated to the

locations described in said protocol. In this step, the ATD limbs can, in CAE, be moved freely around its joints. No contacts are considered, meaning that the ATD will not compress but instead intersect itself or other objects in the environment. To account for this behavior, when the ATD has been positioned, it is recommended by the ATD model manufacturer to use the 'marionette method' to pre-simulate and de-penetrate the ATD (Humanetics Innovative Solutions, Inc., 2019). The method pulls the ATD limbs into position in a simulation using cables, which will ensure that the ATD is intersection free and compressed where the ATD is in contact with itself.

2.5 Numerical reproducability

Software used in crash simulations, such as LS-DYNA, utilizes explicit time integration formulation, due to the highly time dependent and non-linear dynamics of a crash (Schmitt, 2009). The explicit formulation is based upon solving for the kinematics of nodes and scales well when solved using multiple CPUs due to de-coupling of equations compared to implicit formulations (Harish, 2020). Distributing computational workload comes in handy as simulations in the field of crash safety is too large to time-efficiently be solved by a single CPU. For splitting workload and solving parts of the simulation in parallel across more than one CPU, model decomposition is used. The FE model is split into parts and passed to different CPU-cores using the Message Passing Interface (MPI). MPI is a way for multiple CPU-cores to exchange information when running a parallelized simulation or program across distributed memory (Gillis & Bigelow, 2022). It is known that this time-efficient way of running programs often conflicts with the ability to create reproducible results in simulations. Depending on in what order partial calculations arrive from each indivual CPU core and numerical round-off associated, the numerical end result might differ when running the same simulation on a different configuration of hardware and software. Although, running consecutive runs of the same simulation, with identical input data and solver settings on the same hardware will produce the same output (Diethelm, 2011).

3 Method

The work in this thesis was conducted by reviewing literature for occupant positioning methodologies, legal and consumer rating procedures, and analyzing manufacturer specific guidelines for conducting ATD positioning in CAE and ATD de-penetration simulations. The authors created an automated method for ATD positioning, which was validated by comparing its output to physical test data. The positioning procedure takes an ATD model, car environment model as well as user inputs. The implementation of the automated positioning method creates a de-penetration simulation file that can be executed in LS-Dyna.

Two application studies were conducted utilizing the automated positioning for ATD positioning in CAE. Numerical reproducibility of an ATD in a frontal impact load case was assessed. The simulations were conducted using the same High-Performance Computer (HPC), LS-Dyna solver, and MPI version. Furthermore, a parameter study was conducted on how H-point position affects injury criterion in the same frontal load case. The H-point variations were obtained through statistical analysis of physical tests conducted by the car manufacturer.

In this thesis, the car coordinate system has been used. The positive direction of the X-axis refers to rearwards of the car, the Y-axis extend from the left-hand-side to the right-hand-side and the Z-axis extend upwards in the car, shown in *Figure 4*.

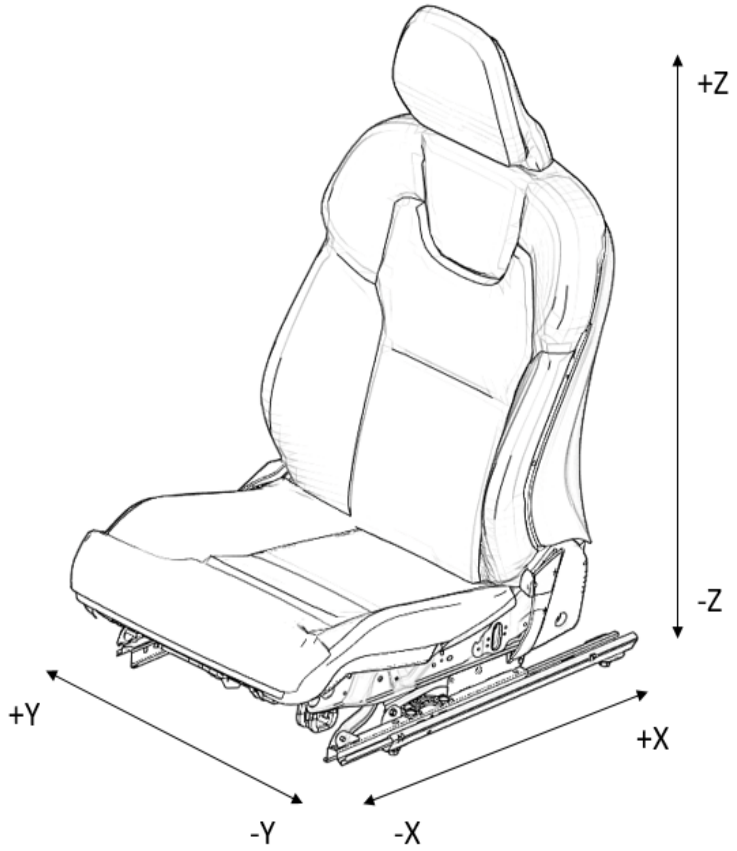

Figure 4: Illustration of car seat in the car coordinate system.

3.1 Development of ATD positioning method

The developed ATD positioning method was implemented using a collection of Python scripts. These scripts make calls upon the simulation model pre-processing software to position an ATD in any of the five available seat positions in a car, according to a chosen protocol. The collection of Python scripts enclosing the automated positioning method with associated support functions are named the implementation of the automated positioning method throughout this report.

ANSA (BETA CAE Systems, Luzern, Switzerland) was used for implementing the automated ATD positioning method. ANSA provides tools for positioning the ATD model, such as kinematic joint rotation, H-point translation, and pre-simulation creation using the Marionette method for force cable generation. ANSA uses Python as its main script language for communicating with its API. Furthermore, ANSA's API allows for automation of model manipulation which was a necessity for choice of model pre-processor.

In *Figure 5* provided below, a flowchart of the implementation of the automated positioning method is shown. Although simplified, the flowchart demonstrates the relation between the functions positioning the ATD and the necessary support functions. As a support function the Graphical User Interface, GUI, aids user operation of the implementation of automated positioning method by providing access to available options and settings. The GUI was also responsible for letting the user pick model attributes that was necessary for the automated positioning method to operate. In addition, the user was allowed to make changes to the final position when the positioning was finished. Finally, the Marionette method creates the ATD pre-simulation.

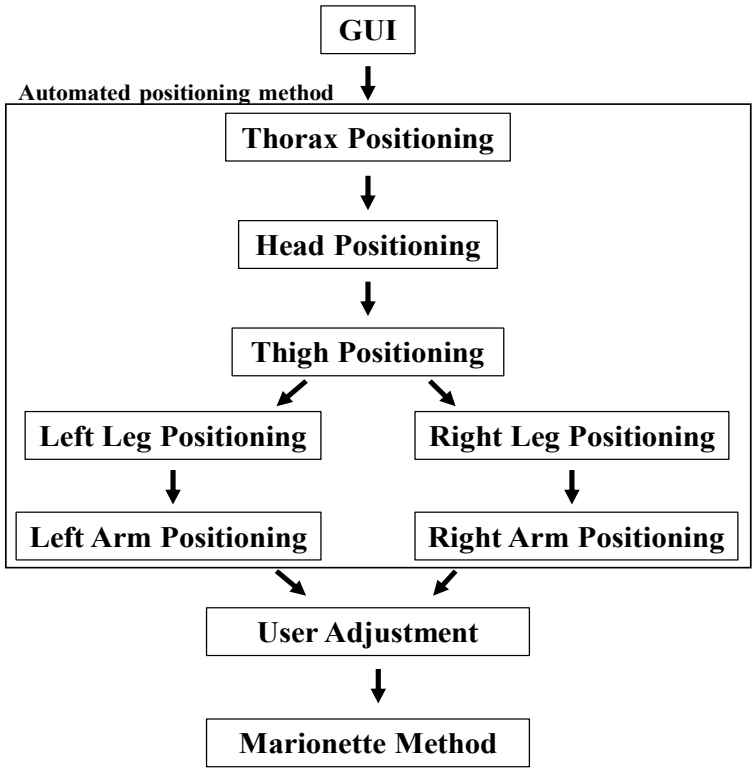

Figure 5: Simplified flowchart of the implementation of the automated positioning method.

3.1.1 General automated positioning techniques

The kinematic joints and bodies of the ATD were connected in a tree structure. Rotating a kinematic joint will relocate all the bodies in the model that was connected downstream that branch of the tree. The 'Dummy Articulation' tool present in ANSA was used within the implementation of the automated positioning method to rotate the ATD's kinematic joints, within the kinematic joints' degrees of freedom, to a desired location.

Two general methods for positioning ATD limbs were used. Firstly, intersection checks, illustrated in *Figure 6*, which refers to detecting interferences or collisions between surfaces in the FE models. Intersection checks was used to position ATD limbs where there were clear environmental constraints that needed to be considered or limited degrees of freedom for the limb.

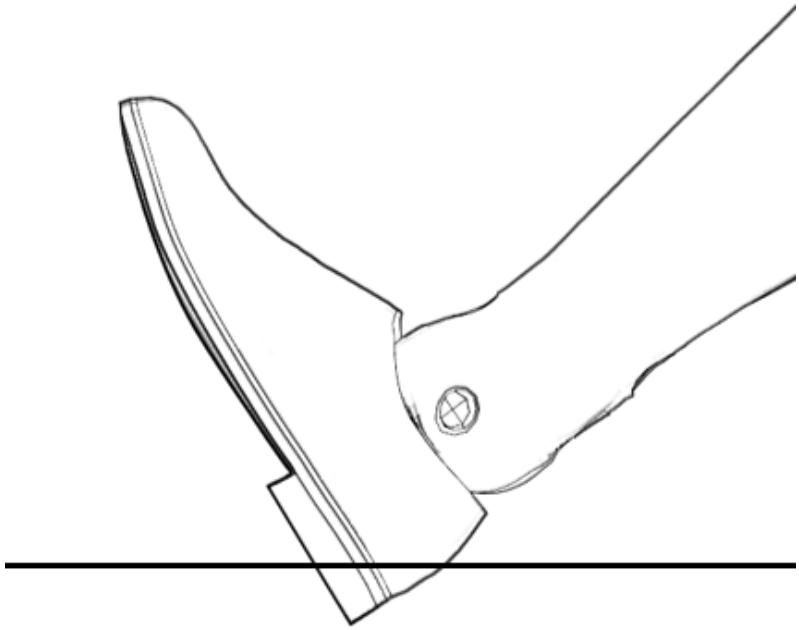

Figure 6: Exaggerated intersection between ATD foot and surface.

When there was more than one degree of freedom or no clear environmental constraints, an optimization algorithm to minimize the distance between nodes was used. For example, driver's hands were positioned using distance minimization. Another use case for distance-minimization was when a specific distance requirement should be met, as was the case for knee-to-knee distance. Although, this method requires nodes to be predefined on the ATD and knowledge about where parts were in the environment to function. This increases workload on the user and lowers the degree of automation, which was why intersection-based positioning was preferred in most cases.

3.1.2 General for all seating positions

In the seat models, the R-point was pre-defined by a marker. The marker location was picked by the user within the GUI and the implementation of the automated positioning method found the coordinates of the middle node of the marker. The ATD's H-point was translated to the coordinate using a user defined H-point offset. Pelvis angle was given within the protocol together with the acceptable tolerance for the specific ATD and load case. The thorax was positioned by intersection checks to the seat backrest and rotating the lower lumbar spine until intersection occurs. The Hybrid III ATDs offer little spine flexibility. As a result, the backrest might not be reached. The head instrumentation board inside the ATDs head was positioned level with the XY-plane. This was accomplished by minimizing Z-axis-distance between nodes located on forward- and rear-most of the instrumentation board while rotating the head around the neck-joint.

3.1.3 First row seating positions

When the ATD had been positioned in the seat, the distance between the knees was positioned. Depending on ATD and test protocol either the CC-distance or the OO-distance between the knee was used, displayed in *Figure 7*. For implementation purposes this information together with the specific distances has been placed in a look-up-table.

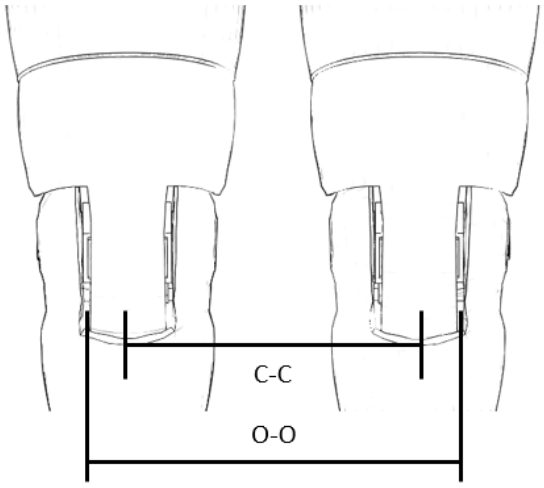

Figure 7: Illustration of Centre-to-Centre (CC) and Outer-to-Outer (OO) distance.

Distance optimization was performed, rotating the hip-joints symmetrically, laterally using decreasing step-size until the correct knee distance was obtained. A decreasing step-size was used to converge to the correct knee distance while keeping the accuracy associated with a smaller step-size.

The automated positioning will then ensure proper intersection between thigh and seat automatically. This was done by rotating the upper leg around the horizontal upper leg joint, shown in *Figure 8*, until intersection between thighs and seat cushion occurs. The implementation of the automated positioning method contains a setting for thigh intersection with the seat cushion. The thighs intersection setting can be used to manually configure how much thigh intersection with the seat cushion is allowed.

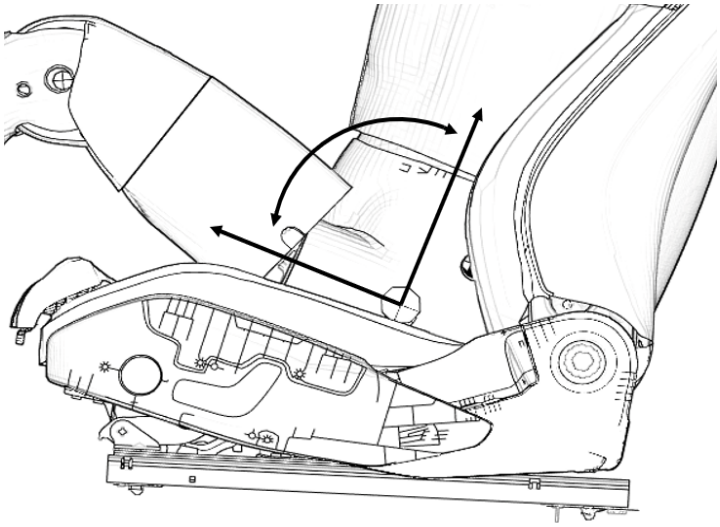

Figure 8: Upper leg rotation around hip-joint horizontal axis

After positioning the upper legs, the lower leg of the ATD was adjusted. The lower leg was rotated around the knee joint, which has only one degree of rotational freedom, shown in *Figure 9*.

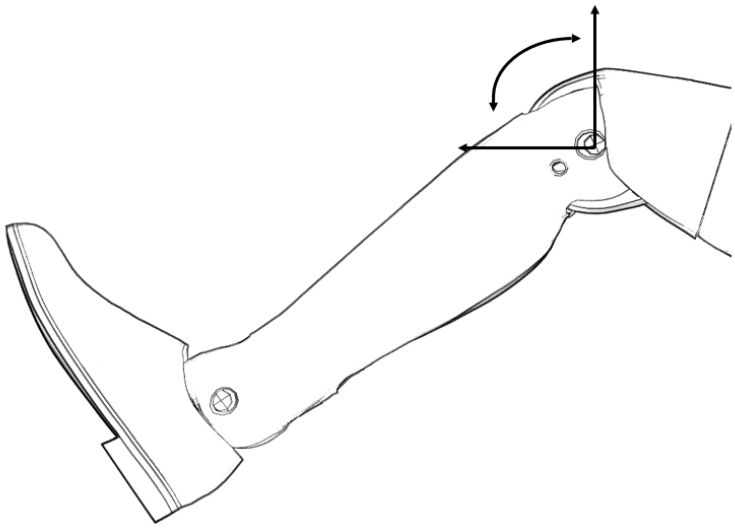

Figure 9: Lower leg rotation around knee joint

The automated positioning method checks that the ATD's foot was located above the carpet and that there were no intersections between the ATD foot and the car environment by raising the lower leg.

3.1.4 Driver feet

The leg was rotated outwards around the hip joint, illustrated in *Figure 10*, until a fictional center plane, which runs through the length of the leg, cuts the accelerator pedal or foot stand in the middle.

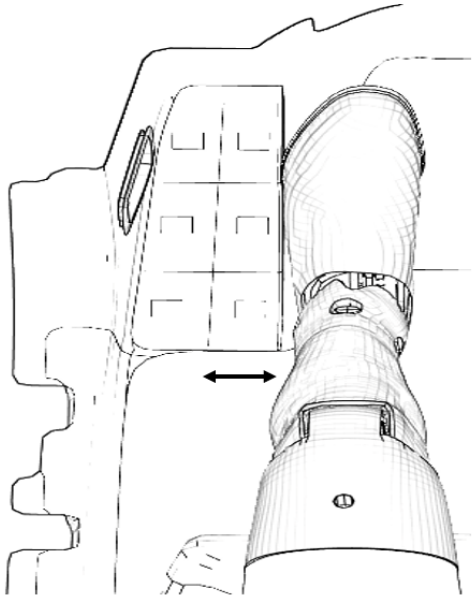

Figure 10: Leg rotation outwards

As seen in *Figure 11*, driver's feet were rotated inward by minimizing the Y-distance between the predefined node on the ball of the ATD to nodes identified by the automated positioning method on the foot stand and accelerator pedal, respectively.

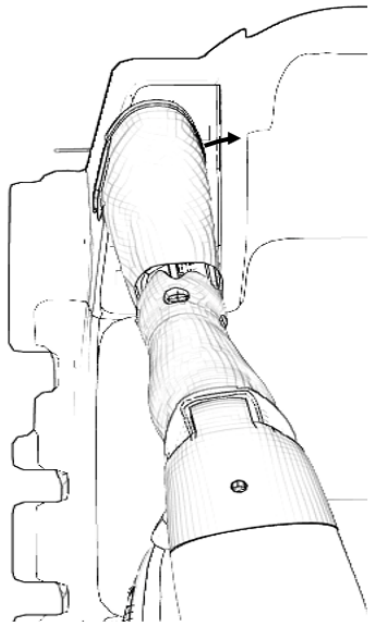

Figure 11: Rotating foot, centre of ball to centre of foot stand

When the Y-distance is within a certain tolerance the feet were rotated downward until intersection occurred between the sole of the feet and accelerator pedal or foot stand and backed off until intersection is no longer present, illustrated in *Figure 12*. In the case that driver's legs do not reach the accelerator pedal or foot stand this step was skipped and the feet were left in their initial position.

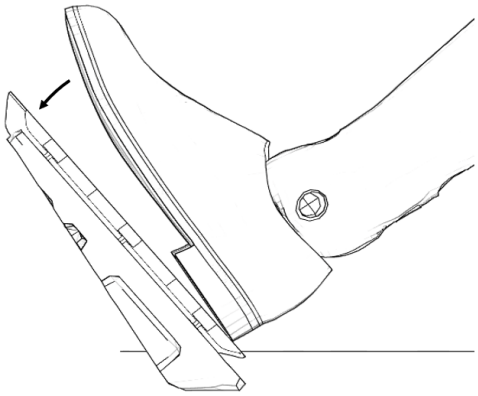

Figure 12: Foot rotated to rest on foot stand.

3.1.5 Passenger feet

The passenger feet were initially rotated inwards to avoid intersection to the walls around the footwell. The feet were rotated downward until intersection occurs between the shoe sole and the carpet, illustrated in *Figure 13*. The feet were rotated upward until intersection no longer occurred.

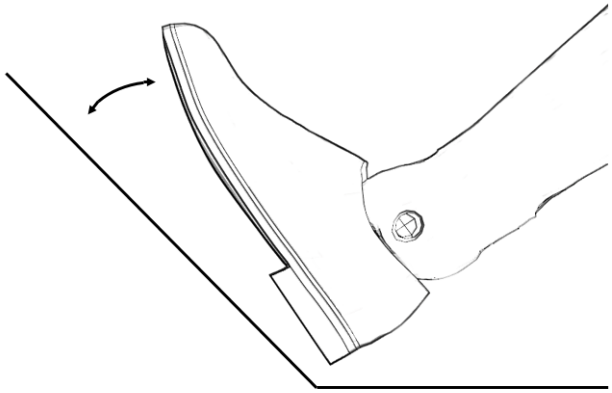

Figure 13: Downward and upward foot rotation.

The passenger feet were rotated outwards around the longitudinal axis, illustrated in *Figure 14*, until intersection occurs between feet and the walls of the footwell, or the foot was pointing straight forward.

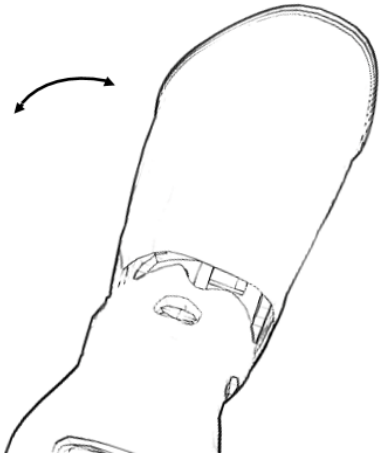

Figure 14: Outward rotation of the foot.

3.1.6 Driver hands

Before positioning the driver hands at nine and three o'clock at the steering wheel, the upper arm angle, demonstrated in *Figure 15*, relative to the thorax were positioned. The upper arm angle was set to leave little room between the upper arm and thorax. With upper arm angle fixed, it limits the total amount of degrees of freedom for the hand movement.

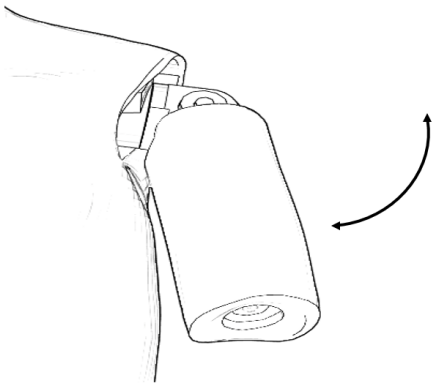

Figure 15: Upper arm angle movement.

The ATD's upper arms were initially positioned straight forward. The distance minimizing search algorithm then minimized the distance between the predefined nodes on the ATD's palms and nodes positioned at nine and three o'clock at the steering wheel. The steering wheel nodes were automatically identified by the automated positioning method.

The optimization algorithm operated using three degrees of rotational freedom. Yoke angle, for regulating X-distance, elbow around the vertical axis for regulating Y-distance and lower arm angle to regulate Z-distance, demonstrated in *Figure 16*. This was done using decreasing rotational step-size making smaller adjustments the closer the palm got to its final position on the steering wheel.

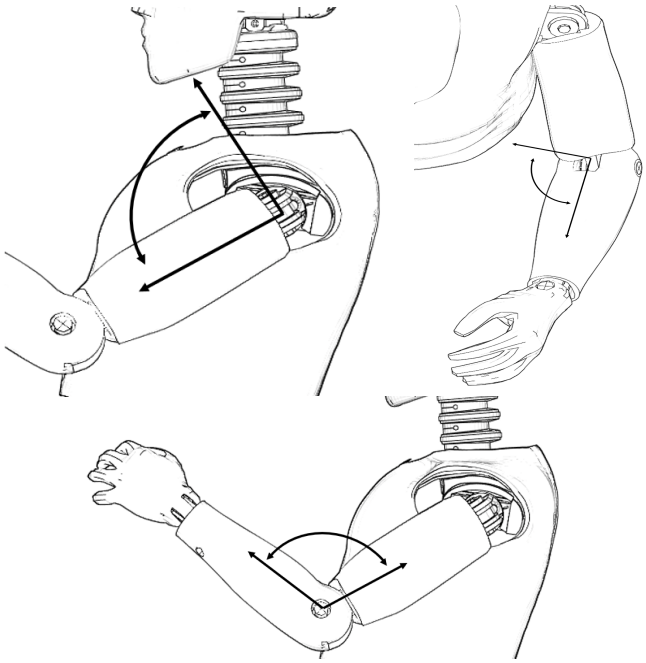

Figure 16: Yoke angle, elbow angle, lower arm angle, respectively.

3.1.7 Passenger arm and hands

The automated positioning method ensured a close fit between the ATD's upper arm and seat backrest by rotating yoke backwards until intersection occurs between upper arm and backrest, illustrated in *Figure 17*. The yoke were rotated forward until intersection no longer occurred. The same method was used regarding the ATD's upper arm and thorax.

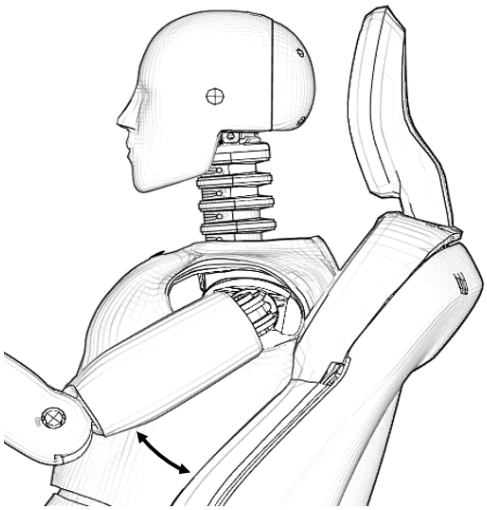

Figure 17: Adjust yoke angle to backrest

In this stage intersection might occur between ATD's hand and thighs or the seat cushion. The lower arms were rotated upwards until intersection no longer occurs. The lower arms were then, iteratively, rotated downward until intersection occurs between ATD's hand and thigh and rotated outwards until the ATD's hand intersected the seat cushion. The lower arms were rotated upwards until intersection no longer occurs which positioned the ATDs hands besides the thighs and above the seat cushion.

3.1.8 General for second row seating positions

The ATD was initially positioned as described in Section 2.1.4, but in a squatting position, as shown in *Figure 18*. The squatting position ensures that there was no initial intersection with floor carpet or first row seat back. Thighs were lowered until the ATD's heels contacted the carpet or intersection occurs between the thighs and seat cushion.

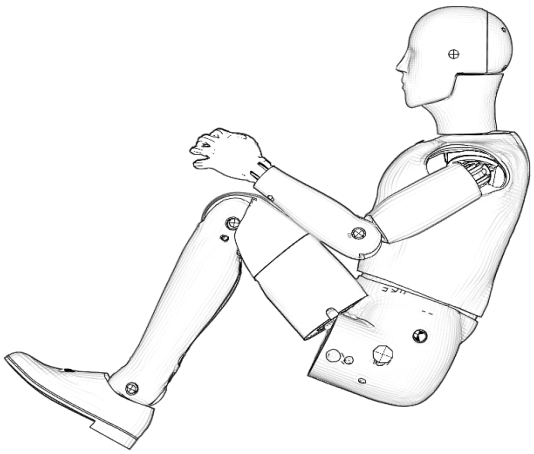

Figure 18: Initial squatting position in second row

The ATD's feet were rotated downward until the sole of the foot contacts the carpet to ensure that the feet were positioned flat to the floor. Iteratively the feet were slithered forward, extending the legs by rotating the lower leg upward while ensuring contact between sole and carpet as well as heel and carpet until the foot contacts the first-row seat back or center console. In the case the ATD's feet do not reach first-row seat back or center console the feet were left flat to the floor.

Arms and hands in second row were positioned similarly to the first-row passenger arm and hands. The upper arm was positioned, by rotating the upper arm backwards until intersection occurs between the upper arm and the backrest. The upper arm was rotated forward until intersection no longer occurs and the upper arm was positioned close to the backrest. The same method was used regarding ATD's upper arm and thorax. In this stage intersection might occur between ATD's hand and thighs or the seat cushion. Lower arms were rotated upwards around the longitudinal axis until intersection no longer occurs. Lower arms were then, iteratively, rotated downwards until intersection occurs between ATD's hands and thighs, and rotated outwards until the ATD's hands intersect the seat cushion. The lower arms were rotated upwards until intersection no longer occurs which will position the ATDs hands besides the thighs and above the seat cushion.

3.1.9 Performance validation of positioning method

The purpose of reconstructing standardized test procedures in CAE is to predict the outcome of physical validation. Therefore, the ATD positioning in CAE should be replicating physical ATD positioning as close as possible. The performance validation was performed by comparing an automatically positioned ATD to ATD coordinates measured in physical tests at the car manufacturer. The assessment was performed on an older car project due to test data availability, using the US NCAP full frontal rigid barrier protocol and the driver's seating position. The ATD positioned in the driver's seating position, according to the protocol, is the 50th percentile Hybrid III which was compatible with the implementation of the automated positioning method. The driver's seating position was chosen as it includes both general positioning techniques and was the most technically difficult, in terms of environment interactions. The automatically positioned ATD was positioned using the H-point offset for the 50th percentile Hybrid III in CAE estimated by the car manufacturer. The coordinates compared to physical tests was head CoG, nose-tip, left shoulder joint, H-point, left center of knee-joint and the backmost point of the left heel. The mentioned nodes used for measuring is visualized in *Figure 19*.

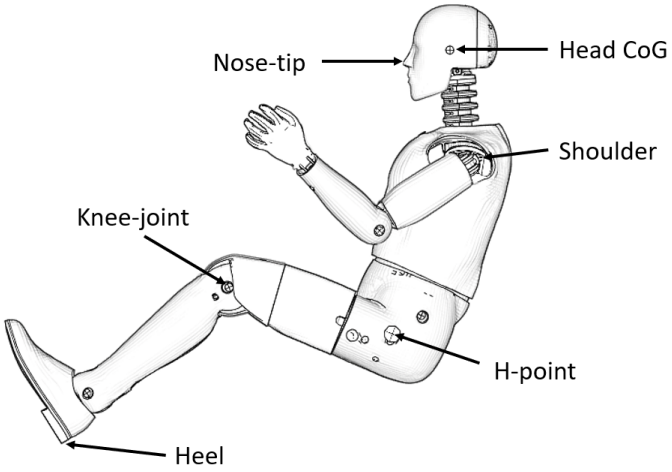

Figure 19: Demonstration of measuring nodes for validation of ATD positioning.

Normality of the physical ATD positioning data was checked using the Shapiro-Wilk test (Malato, 2023) at the five percent significance level and the mean and standard deviation of X- and Z- coordinates was calculated for each measurement location, respectively. Y-coordinates was disregarded, as internal recommendations at the car manufacturer regarding physical ATD positioning had changed since the release of the car model in question, making the comparison for knee and heel Y-coordinate irrelevant.

The measurements taken on the automatically positioned ATD was then compared to the physical test data to give an indication of the automated positioning methods performance. The comparison was made using the resulting ATD model positioning before pre-simulation was conducted. Coordinates located within two standard deviation of the measurements from physical positioning were deemed to be acceptable as they were positioned within approximately 95% of the positions seen in physical ATD positioning. Coordinates located within one standard deviation of the measurements from physical positioning were deemed to be good, reflecting approximately 68% of physical tests closest to the mean positioning.

3.1 Application studies: Injury Criteria variation

Two application studies were conducted investigating variations in ATD injury criteria caused by model decomposition and sensitivity to variations in ATD H-point positioning. The ATD H-point positions used in the second application study was based upon the statistical analysis conducted for the performance validation of the automated positioning method, retrieved from physical tests.

The studies were conducted using a sled model of a mid-size SUV and the 50th percentile Hybrid III ATD. The simulations were setup according to the US NCAP Full Frontal Rigid Barrier 35mph protocol, corresponding to the positioning data from physical tests. The load case exposes the car to a change in velocity of approximately 64 km/h including the rebound from the rigid barrier (Hershman, 2001). The sled model was equipped with steering-wheel-airbag and pre-tensioned, load-limited seatbelt as well as a knee-airbag.

The simulations were all run on a distributed HPC at the car manufacturer equipped with Intel Xeon Gold 6346 CPUs together with Platform MPI v9.1.4.3. For all the

simulation, in both studies, the control card *CONTROL_MPP_DECOMPOSITION_TRANSFORMATION with the flag SX was used. This setting has been shown to be beneficial to decrease simulation time in frontal load cases (Kondo, 2012), and will decomposition the model in slices longitudinally (LSTC, 2007). In *Figure 20*, the model decomposition of the nominal simulation using 160 CPU cores is illustrated. The colored chunks represent how the numerical workload was distributed among CPU cores.

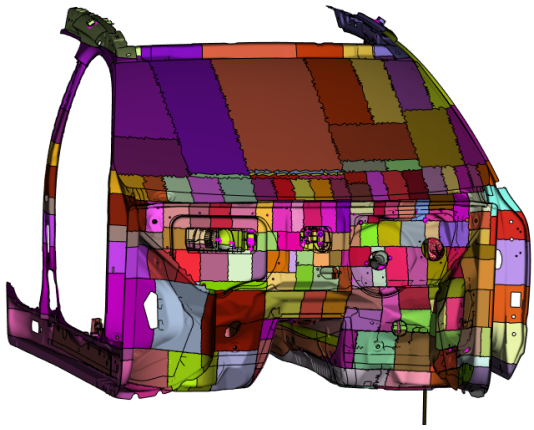

*Figure 20: Illustration of model decomposition using *CONTROL_MPP_DECOMPOSITION_TRANSFORMATION with the flag SX and 160 CPU cores.*

All the ATDs were positioned using the automated positioning method and the belt was routed manually for each individual ATD H-point position. Six injury criteria, included within the US NCAP full frontal rigid barrier 35 mph protocol, was assessed: HIC_{15}, N_{ij}, neck tension and extension, chest deflection and femur force.

Injury criteria were calculated using a postscript developed at the car manufacturer using the post-processing software Meta (BETA CAE Systems, Luzern, Switzerland). The injury criteria values shown in the results have been normalized showing only the difference in injury criteria relative the nominal H-point position simulated using 160 CPUs.

3.1.1 Model decomposition

For studying the variation due to model decomposition, the number of CPU cores used was varied from 130 to 190 in steps of ten, resulting in seven simulations. Varying the number of cores will result in different model decomposition as the numerical workload will be distributed differently across the CPU cores (Diethelm, 2011). The H-point position used for studying model decomposition was using the mean X and Z H-point coordinates found in the physical test data.

Östh et al. (2021) found that numerically induced noise behaved randomly with the number of CPUs. Therefore, the injury criteria values were assessed in terms of CV. The CV is the standard deviation of injury criteria, σ, divided by the mean, μ, shown in *Equation 3*:

$$CV = \frac{\sigma}{\mu} \qquad (3)$$

3.1.2 H-point positioning

For studying sensitivity to H-point variations the number of CPU cores were kept constant at 160 cores. In *Figure 21*, the H-point positions measured is represented with black dots. The H-point positions chosen, for the study on injury criteria variations due to H-point variation, were the intersection points between the standard deviation lines in X- and Z-direction. The covered H-point area in the XZ-plane is marked using white. Hence, one H-point position found in physical testing, is contained within the grey marked area.

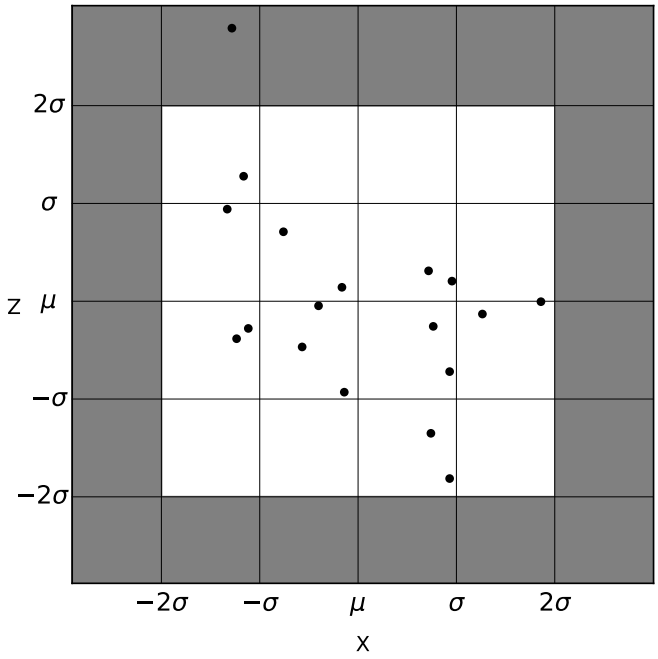

Figure 21: Scatter plot of H-point positions measured in physical tests, represented with black dots.

Furthermore, the nose-to-belt distance, shown in *Figure 22*, was measured for all H-point positions. The nose-to-belt distance was measured as the Z-direction distance from the most outer node of the nose-tip to the lowermost part of the shoulder belt, where the belt crosses the sternum.

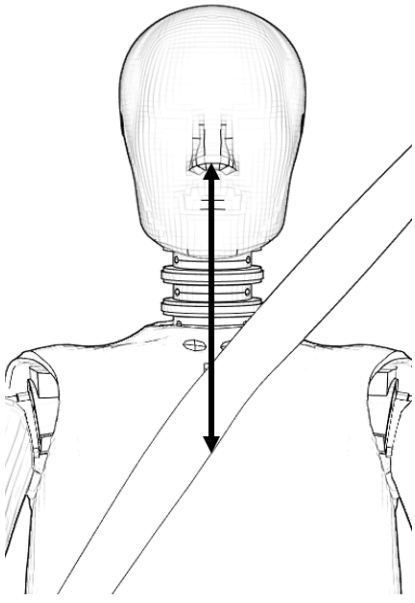

Figure 22: Illustration of nose-to-belt distance.

4 Result

Here the implementation of the automated positioning method is described, and the performance is reported. Furthermore, the results from the two application studies on numerical reproducibility due to model decomposition and global injury criterion variation due to H-point movement is included.

4.1 Automated ATD Positioning

The implementation of the automated positioning method developed could position the three adult Hybrid III ATDs in the car platforms used for development of the method, although with some limitations. Depending on which position, ATD and complexity of car environment model the positioning script took between 5-10 minutes to run. The user operates the implementation containing the method by giving input through a graphical user interface.

When the implementation of the automated positioning method has finished the initial positioning, the user was allowed to make changes to the ATD position before a pre-simulation file was created and ATD coordinates was saved. The pre-simulation was created using the Marionette method within ANSA automatically.

4.1.1 Model prerequisites

There were prerequisites for the automated positioning method to function. The method required a car environment which consisted of a seat, pre-positioned for the ATD and test protocol, as well as the close surroundings of the ATD such as floor carpet. Additionally, models of a steering wheel and pedals were required for positioning the driver. As for passengers in the second row, front seats and tunnel console was required.

ATD model kinematic joints needed to follow a standardized naming scheme, as was the case regarding the ATD contact surfaces. This was for the automated positioning method to be able to position any of the Hybrid III ATDs. Due to the possibility of ATD model part and joint naming inconsistencies over the variety of compatible ATDs, a conversion script was developed for this project to unify the ATD naming of parts and joints.

The automated positioning method took advantage of named nodes, used for measuring distances. Named nodes were used to increase ATD model compatibility as node-id numbering can change due to several reasons such as, model changes or node-id conflicts which might lead to automatic renumbering done by the pre-processing software. The nodes named for positioning the Hybrid III ATDs were located at the palm of the hands, backward most nodes of the heels, ball of the feet as well as backward most and forwardmost node on the head instrumentation board.

4.1.2 Implementation

The graphical user interface takes input from the user and passes it on to the script containing the method. Here a user can pick which seat to position the ATD in, which ATD to position, which protocol to use, a desired H-point offset, Hip-angle as well as a file path to a file containing the car environment and a destination path for creating the simulation file for ATD de-penetration. If the chosen seating position is not driver, the user can choose whether the hands should be placed on or on the side of the ATDs thighs. *Figure 23* below illustrates the Graphical User Interface.

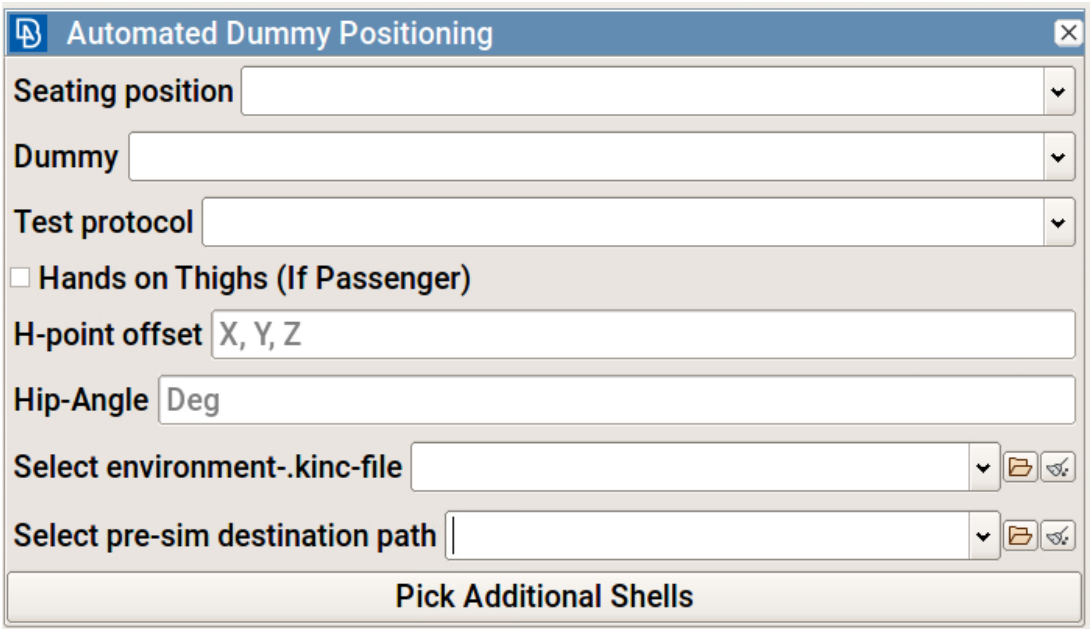

Figure 23: Graphical User Interface

When the user press on 'Pick Additional Shells', the user inputted car environment is loaded. The user is prompted to pick out parts in the car environment model that the method needed information about as for they were located. Except for when positioning an ATD in the driver's position, the only entity that needed to be given was the R-point marker in the seat. In the case of positioning the driver, the script also required the faces of accelerator pedal, foot stand and steering wheel. Due to the possibility of more than one R-point markers contained in the seat model and naming inconsistencies of parts in models this was not automated. When the ATD positioning has finished, it saves the coordinates of the measurement nodes described in Section 2.2 as documentation of the positioning as well as creates a pre-simulation using the marionette method.

4.1.3 Positioning Hybrid III fifth percentile female

The smallest of Hybrid III ATDs, the fifth percentile female, could be positioned using the automated positioning method, to any of the five seating positions taken into consideration. However, it did not always reach the designated feet positions, when the seat was positioned in the manufacturers designated design position for the fifth percentile Hybrid III ATD. Protocols have exceptions of how to place limbs if they do not reach the designated position, although this is still to be implemented within the method.

In *Figure 24* below the fifth percentile has been positioned using the automated positioning method according to the EU NCAP protocol. As seen, the hands have been positioned at 9 and 3 o'clock, thorax aligned with the seat backrest and head instrumentation board parallel to the X-axis in the car coordinate system. Since the feet did not reach the designated feet positions at the foot stand and accelerator pedal, the knee distance has been set according to protocol, and feet left unchanged. Fifth percentile Hybrid III ATD driver, positioned according to the US NCAP protocol, positioning was similar. The main dissimilarities being different knee-to-knee distances and differences in the designated seating position for fifth percentile Hybrid III ATD for the different NCAP frontal protocols.

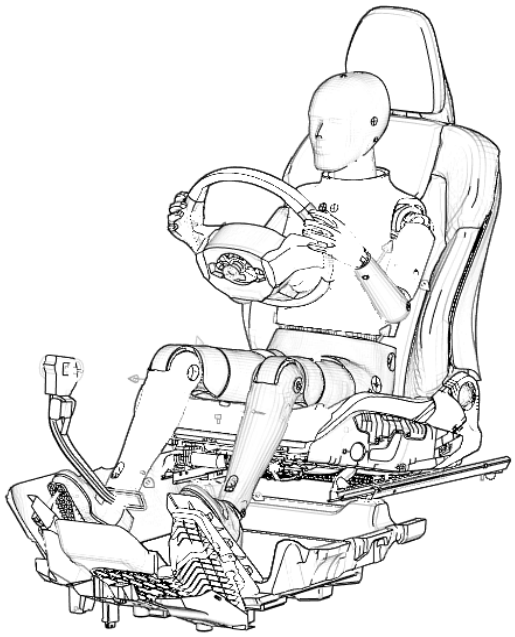

Figure 24: Hybrid III fifth percentile positioned in driver seating position according to the EU NCAP protocol.

Regarding first row passenger positioning for the fifth percentile Hybrid III ATD, again the legs were not long enough to reach the footwell footrest, and the knee-to-knee distance set according to protocol and feet left unchanged with the feet pointing straight upward-forward, as seen in *Figure 25*. The hands were automatically positioned besides the thighs as requested by the operator.

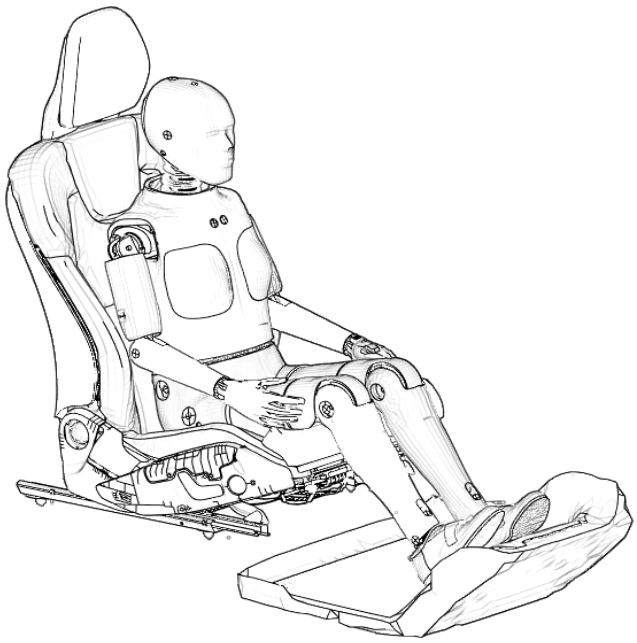

Figure 25: Fifth percentile Hybrid III female positioned in passenger seat.

The fifth percentile Hybrid III, second row passenger, has fewer exceptions. In some cases, the fifth percentile feet did not reach the floorboard. In *Figure 26* below the final position of the fifth percentile Hybrid III ATD in the left, second row seating position is presented. In this instance with the hands positioned on the thighs as requested by the operator.

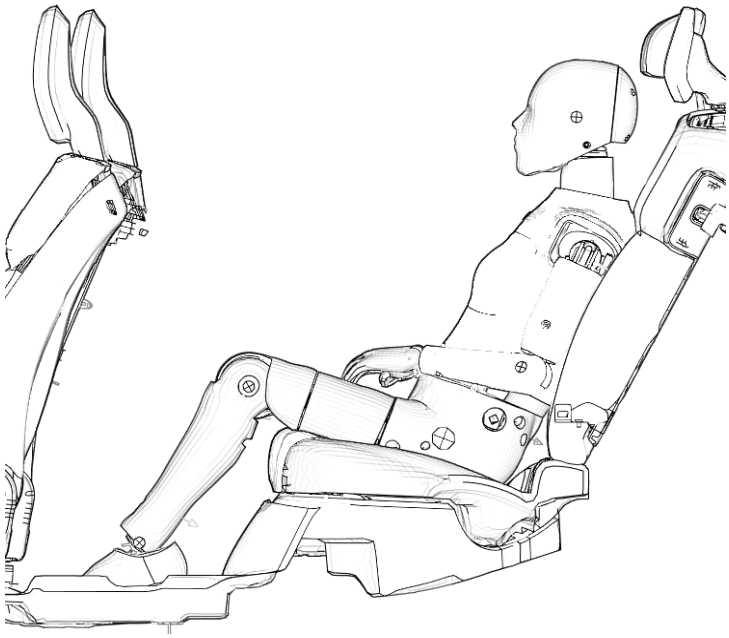

Figure 26: fifth percentile Hybrid III female in left, second row seating position.

4.1.4 Positioning Hybrid III 50th percentile male

The Hybrid III 50th percentile ATD limb length and designated design seat positions were more compatible than for the fifth percentile, which means that in the car models used in development, no protocol exceptions were needed to be made. The better compatibility in relation to the other ATDs considered led to more controlled and better repeatability of ATD positioning.

In *Figure 27* the final positioning, before pre-simulation, of the 50th percentile driver according to the US NCAP protocol is shown. The center plane of the legs intersected the middle of the foot stand. The heels were placed near the intersection of where the fictional plane of the accelerator pedal or foot stand face intersect the floorboard and the feet rotated so that the toes were in line with the center of the foot stand or the accelerator pedal. Hands were positioned with the palm at nine and three o'clock on the steering wheel.

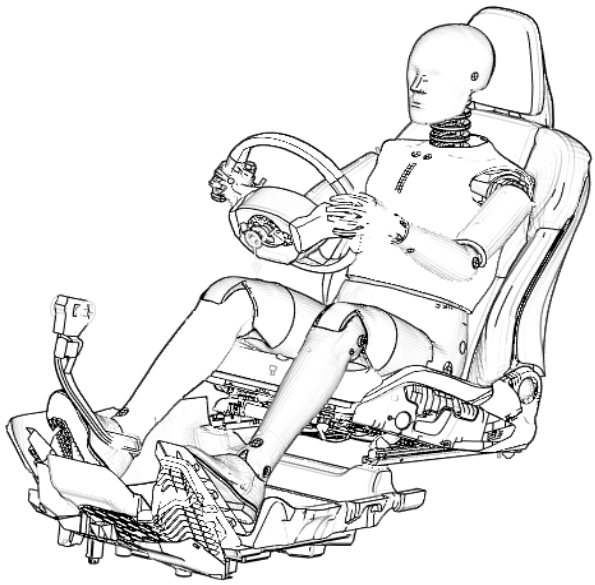

Figure 27: Hybrid III 50th percentile positioned in driver seat according to the US NCAP protocol.

The final position, according to EU NCAP protocol, of the 50th percentile Hybrid III ATD can be seen in *Figure 28*. The thighs were positioned with the knee-to-knee distance according to protocol. Heels were positioned close to the intersection of the footwell footrest and floorboard. Feet resting on the footrest with the right foot slightly rotated inward to avoid intersection with the footwell lining. Hands were positioned by the side of the thighs as requested by the operator.

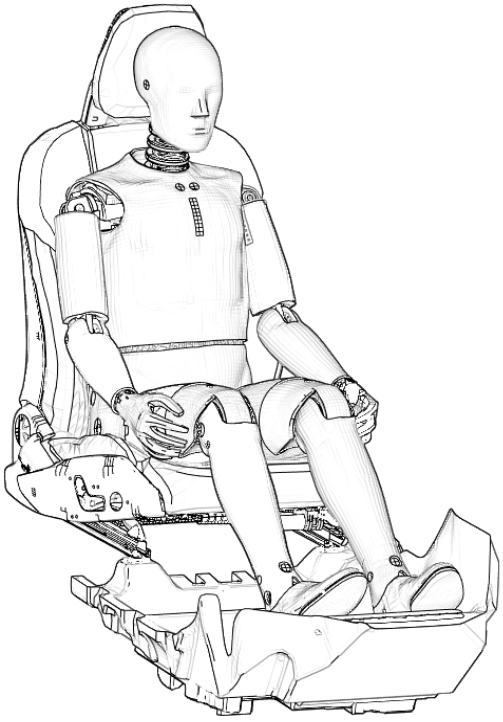

Figure 28: Hybrid III 50th percentile male positioned in passenger seat according to the EU NCAP frontal impact procedure.

Regarding 50th percentile Hybrid III ATD positioning in second row, the feet were positioned flat to the floor, pushed in as far under the first-row seat as possible. This has been done while assuring the final feet position was intersection free, shown in *Figure 29*, a procedure that is hard to perform manually. Hands have been positioned on the thighs as requested by the operator in this case.

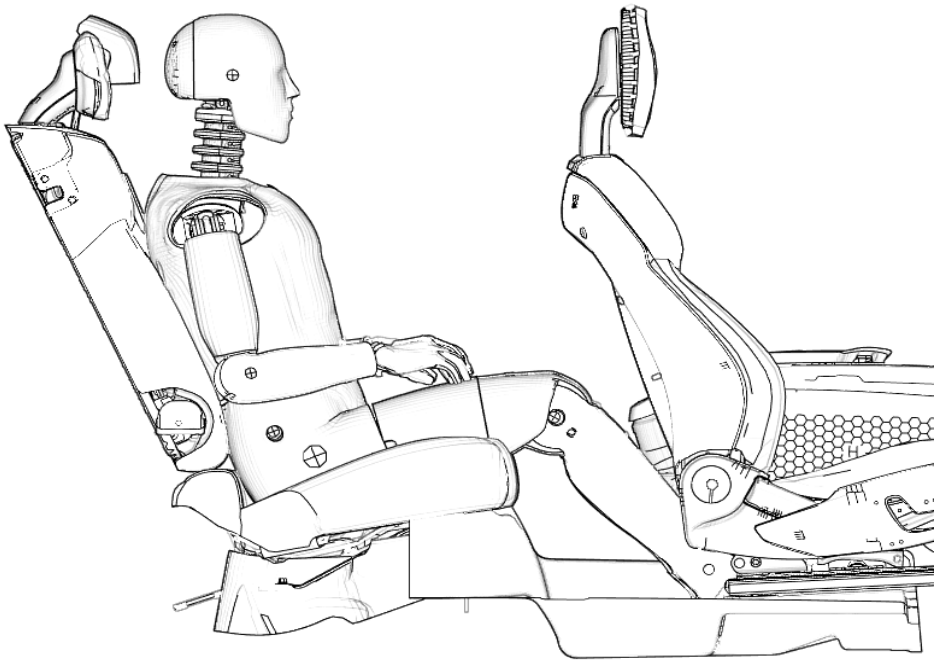

Figure 29: Hybrid III 50th percentile positioned in second row right seating position.

4.1.5 Positioning Hybrid III 95th percentile male

In contrast to the fifth percentile Hybrid III ATD, the 95th percentile can be hard to position due to its large size, especially in the second row in smaller cars. Problems that could occur was knee-intersection with first row seat backrest, among other. In first row, passenger feet positioning performance was dependent on how far forward the seat was positioned due to method lacking function for raising the thighs if the feet were intersecting the footwell using the initial amount of thigh intersection in passenger seat. Feet positioning regarding the 95th percentile Hybrid III ATD in the driver seat was more precise, as the implemented function of node-to-node distance minimization for the driver feet allows for more positioning adjustments.

In *Figure 30*, the final position of the 95th percentile Hybrid III ATD in the driver seat can be seen.

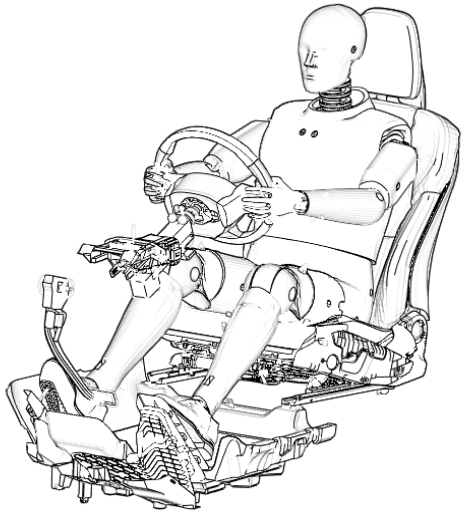

Figure 30: Hybrid III 95th percentile male positioned in driver seat.

For first row passenger positioning using the 95th percentile Hybrid III ATD, which can be seen in *Figure 31* below. Like positioning the 50th percentile Hybrid III ATD, the heels were positioned close to the intersection of the footwell footrest and floorboard, and feet were resting on the footrest with the right foot angled slightly inward to avoid intersection with the footwell lining. Hands have been positioned besides the thighs as requested by the operator.

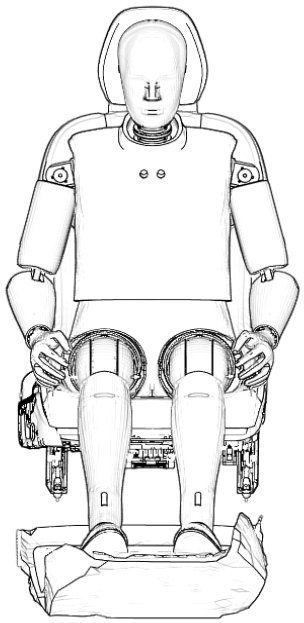

Figure 31: Hybrid III 95th percentile male positioned in passenger seat.

Regarding second row positioning, the Hybrid III 95th percentile ATD is large, this can lead to issues. The ATD knees intersecting with the car environment, feet missing the carpet thus no intersection detected or feet intersecting with procedure terminating objects before getting into position. Although, problems were mostly concerning smaller car models. In *Figure 32*, the 95th percentile Hybrid III ATD has been positioned in one of the car manufacturers mid-size SUV models. The procedure and final position were similar to what was described regarding the 50th percentile Hybrid III ATD above.

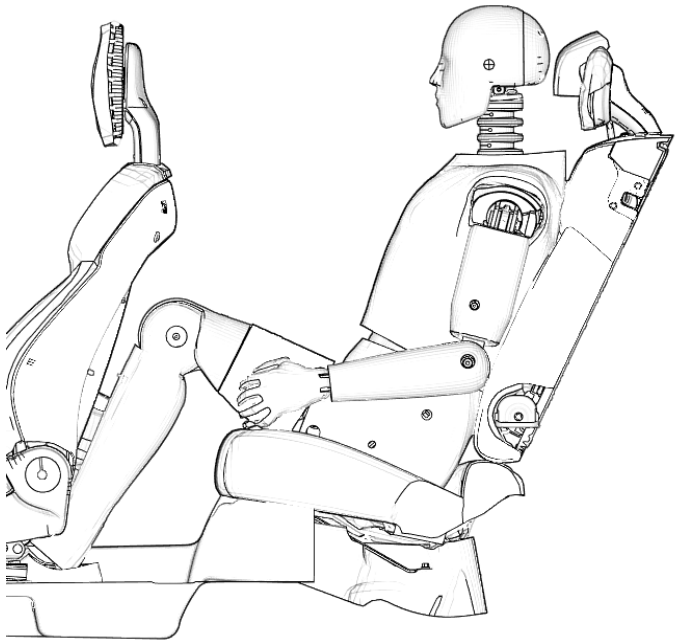

Figure 32: Hybrid III 95th percentile male positioned in the left-hand-side second row seating position.

4.1.6 Performance validation

In this chapter the result of the performance validation of the automated positioning method is presented. For the comparison between physical measurements and the automated positioning method, six ATD coordinates was used in X- and Z-direction. Ten out of twelve sets of measurements had a Gaussian distribution at the five percent significance level. The physical ATD measurements for nose in X-direction and heel in Z-direction did not have a Gaussian distribution at the five percent significance level.

In *Figure 33* below, the 50th percentile Hybrid III male, positioned in the driver's seating position using the automated positioning method was compared with the 18 physical ATD measured. The measured coordinates for the ATD model are connected by the red line, and the physical ATD measurements are connected by the black lines. As seen in the figure, the automated positioning method has positioned the ATD model within the clusters formed by the physical ATD measurements for five out of six coordinates in the XZ-plane. The measured knee-coordinate for the automatically positioned ATD was positioned outside of the spread found in physical testing.

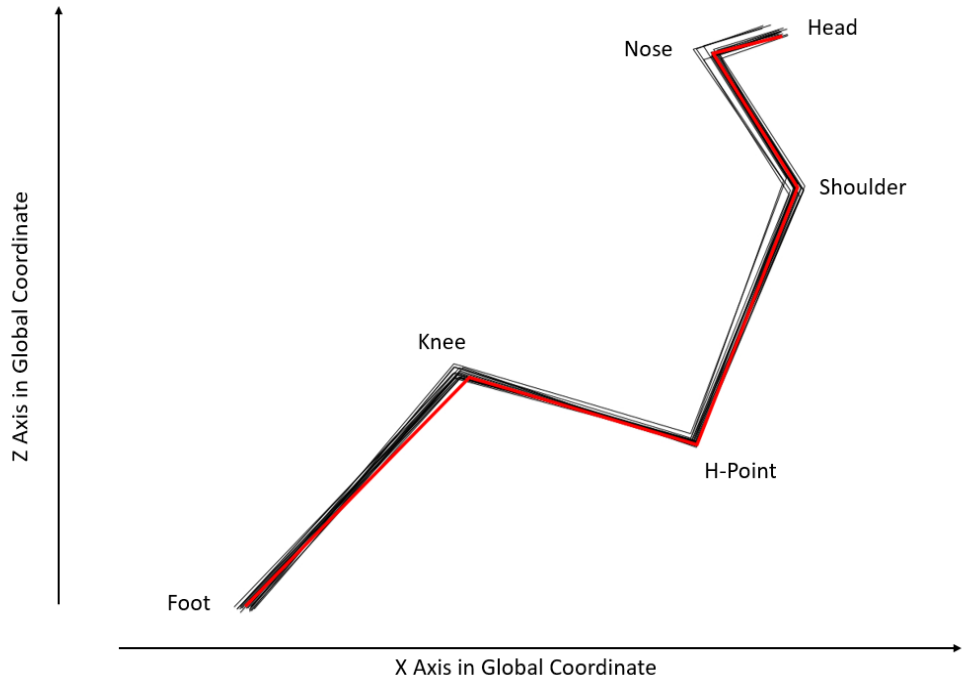

Figure 33: CAE and Physical measurements of 50th percentile Hybrid III in driver's position.

Figure 34 shows the H-point X- and Z-coordinate distribution for the physical ATD measurements, respectively. The red lines represent the probability density function. The red dashed lines, μ, was the mean of the dataset and the thin black lines separated from the median with steps of the standard deviation, σ. The black dashed and dotted lines represent the H-point X- and Z-coordinate of the positioned ATD in CAE, positioned on the R-point using the H-point offset for CAE estimated by the car manufacturer.

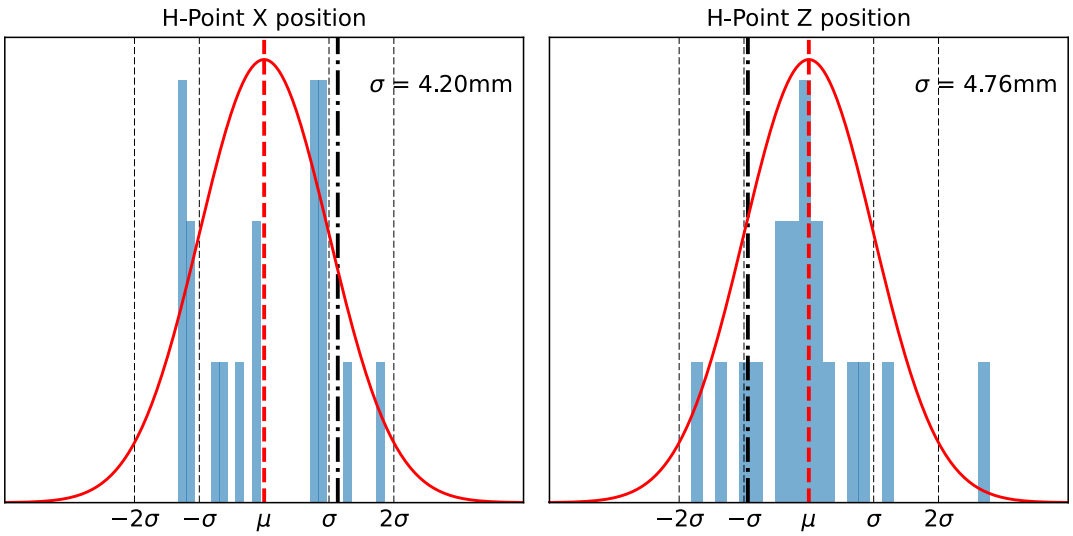

Figure 34: H-point X- and Z-coordinate from physical testing compared to CAE. Red, dashed vertical is the physical test mean and the dashed and dotted black line the CAE position.

Figure 35 below shows a scatter plot of the physical ATD H-point positions, in black, compared to the CAE estimated H-point position, shown in red. The estimated H-point position in CAE was located over one standard deviation away from the median in the positive direction, backwards in the car. As for Z-coordinate, the H-point was positioned approximately one standard deviation below the mean of the data set obtained from physical testing, i.e., lower in the seat.

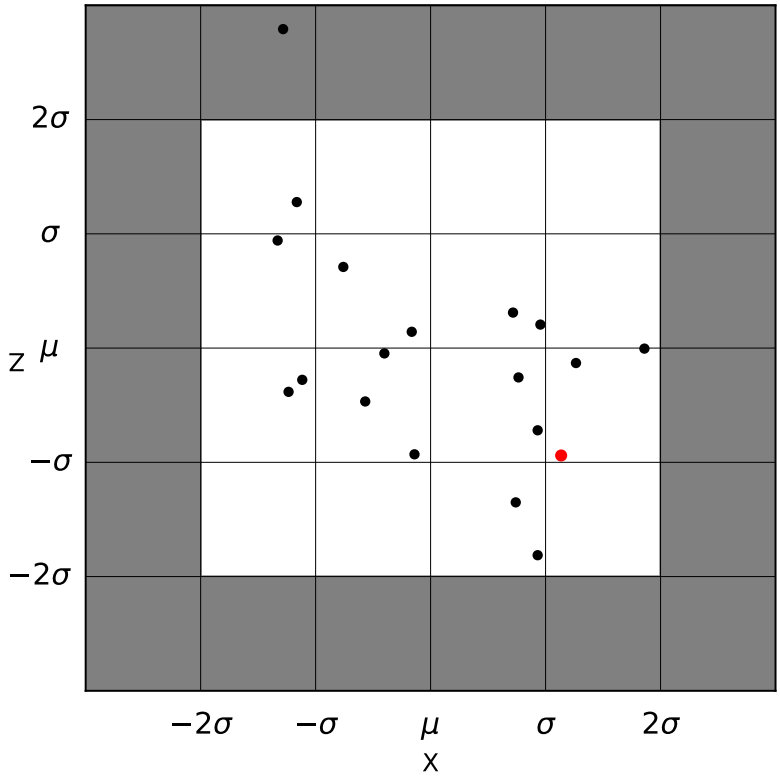

Figure 35: Scatter plot of the physical H-point positions, shown in black, compared to the CAE estimation, shown in red.

The head variation from physical testing compared to the automatically positioned 50th percentile Hybrid III ATD is displayed in *Figure 36* and *Figure 37*. As shown in *Figure 36*, the X-coordinate was located less than one standard deviation backward of the mean in the dataset from physical testing while the Z-coordinate was positioned more than one standard deviation below the mean.

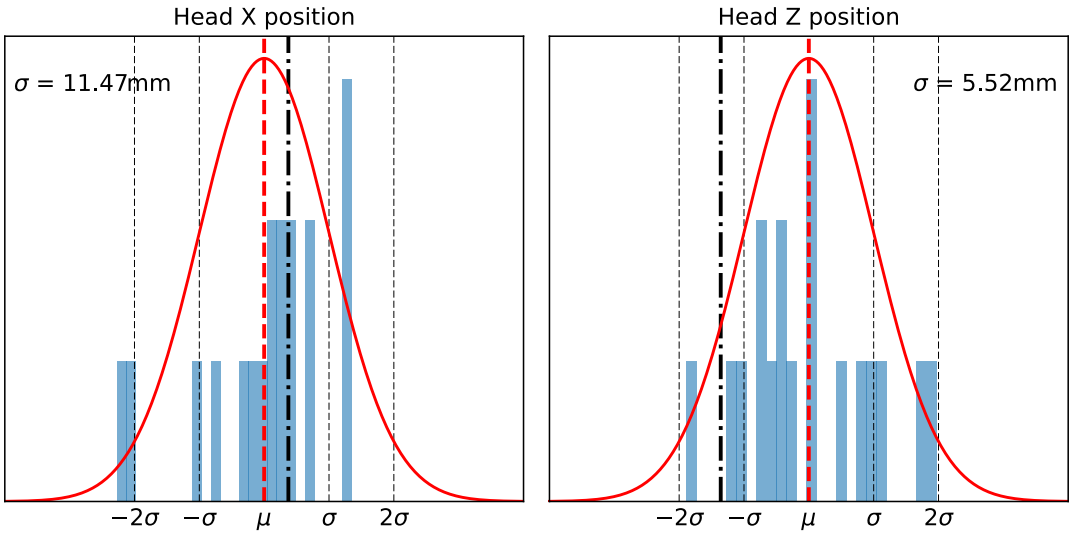

Figure 36: Head X- and Z-coordinate variation from physical testing compared to CAE. Red, dashed vertical is the physical test mean and the dashed and dotted black line the CAE position.

Figure 37 is a scatter plot of the same data points, to give a better understanding of not only the statistics, but visually where the head was positioned relative to the physical ATD measurements. The physical measurements are represented in black, and the measurement taken on the automatically positioned ATD in red. In the physical positioning data of the head, most of the data points form a cluster, although with some data points further forward, in the top-left.

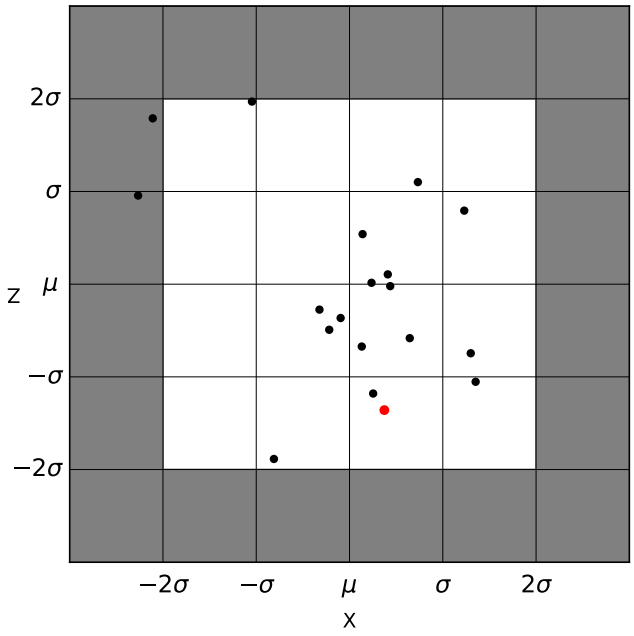

Figure 37: Scatter plot of ATD head position from physical positioning data, in black, compared to the automatically positioned ATD, in red.

In *Figure 38*, the nose X- and Z-coordinates from physical ATD positioning is compared to the automatically positioned ATD. As seen, both the X- and Z-coordinate are positioned close to the mean.

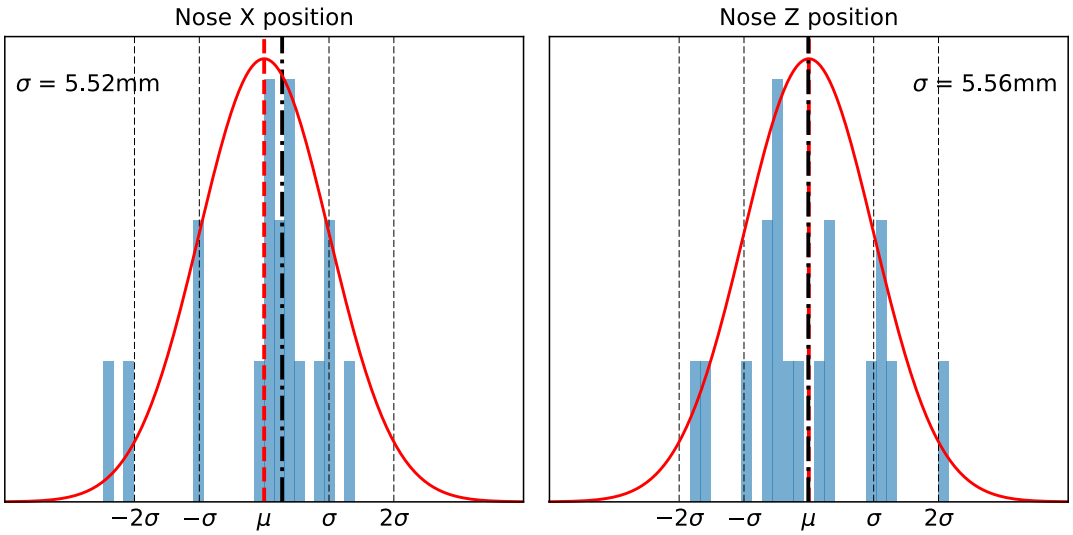

Figure 38: Nose X- and Z-coordinate variation from physical testing compared to CAE. Red, dashed vertical is the physical test mean and the dashed and dotted black line the CAE position.

Figure 39 is a scatter plot of the same data points, giving a better understanding of how the automatically positioned ATD was positioned relative to the physically positioned ATDs in the XZ-plane. The physical head positioning coordinates are represented in black and the automatically positioned ATD's head coordinate represented in red. In *Figure 39*, most of the coordinates are positioned in a cluster, although with some of the points positioned outside of the lines representing two standard deviation distance forward of the mean, in the top-left corner.

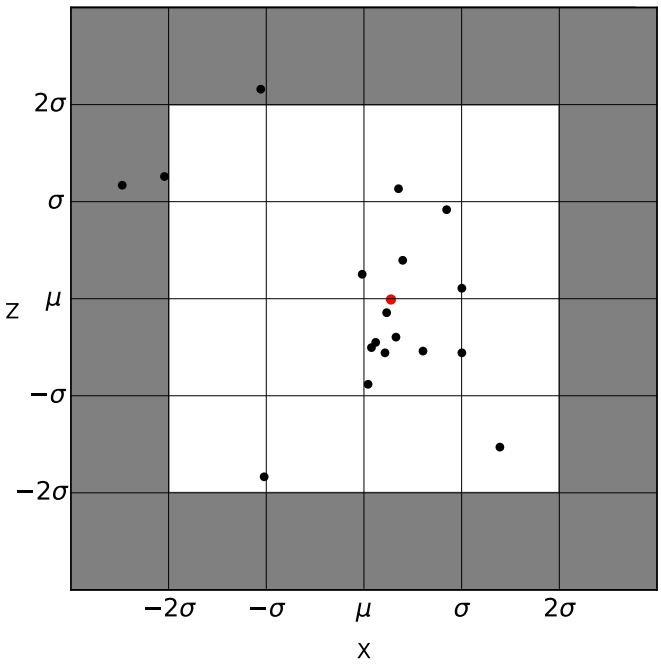

Figure 39: Scatter plot of ATD nose position from physical positioning data, in black, compared to the automatically positioned ATD, in red.

The automated positioning method positions the shoulder X- and Z-coordinate of the 50th percentile Hybrid III ATD slightly above the mean shoulder position obtained in physical testing, as displayed in *Figure 40*.

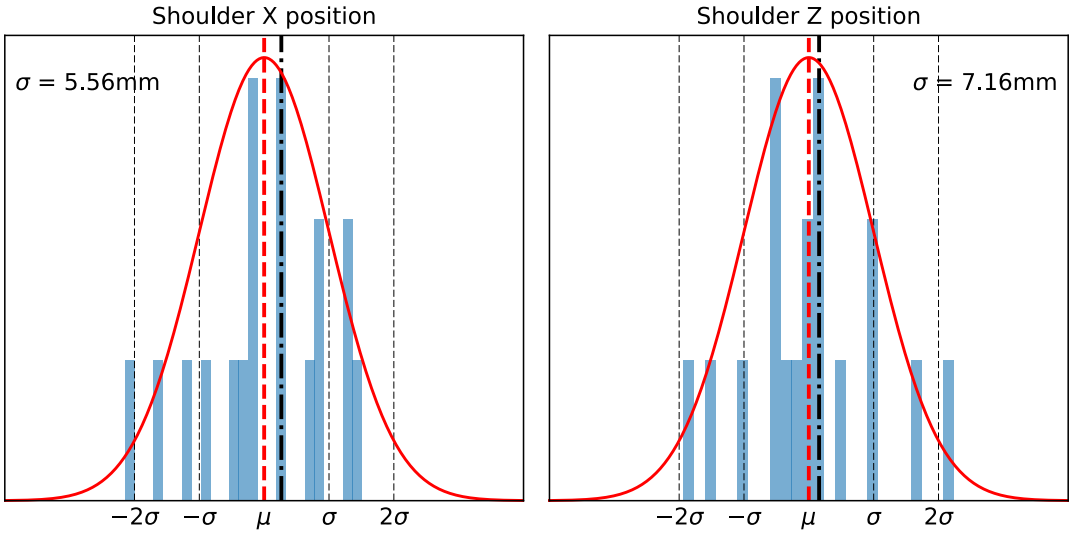

Figure 40: Shoulder X- and Z-coordinate variation from physical testing compared to CAE. Red, dashed vertical is the physical test mean and the dashed and dotted black line the CAE position.

In *Figure 41*, the shoulder positioned is shown as a scatter plot. The shoulder coordinates from physical positioning are shown in black and the automatically positioned ATD in CAE is shown in red. Like what can be seen for nose and head, there is physical coordinates located in the top-left corner.

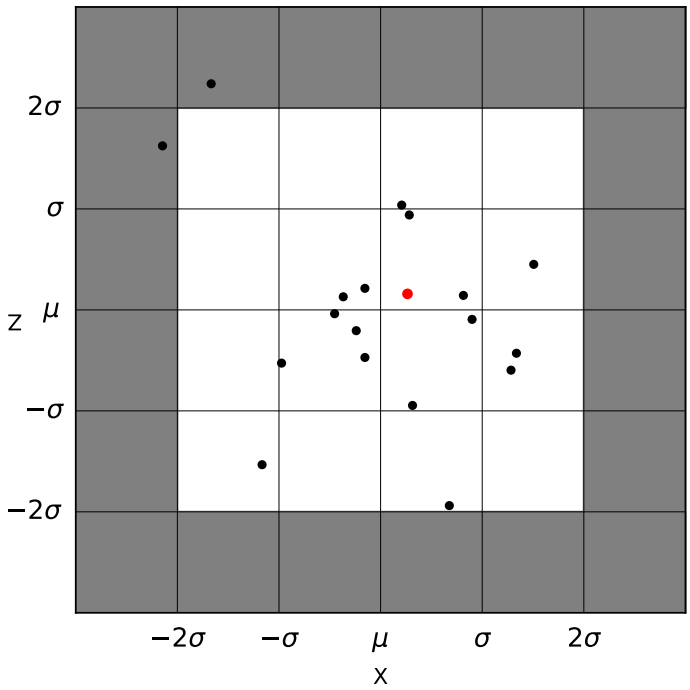

Figure 41: Scatter plot of shoulder coordinates from physical positioning, shown in black, compared to the automatically positioned ATD, shown in red.

The knee positions obtained from the automated positioning method deviated the most of all the measurements from the mean location in physical positioning data, in terms of standard deviation. As shown in *Figure 42*, the X-coordinate of the knee deviated by more than three standard deviations from the mean X-coordinate in physical testing. By reviewing the Z-coordinate, one can see that it was in the lower end of the physical positioning data, positioned one standard deviation below the mean.

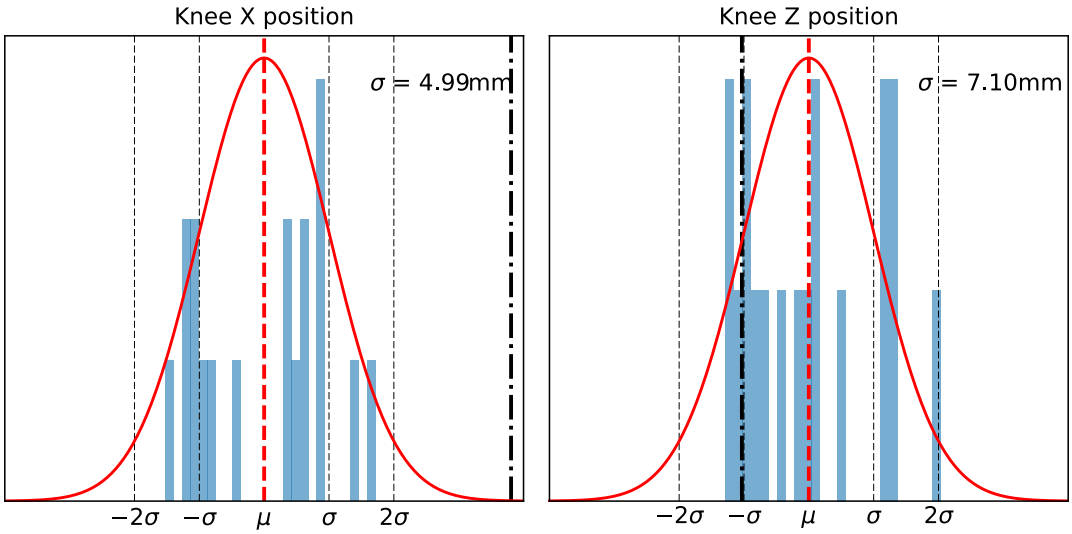

Figure 42: Knee X- and Z-coordinate variation from physical testing compared to CAE. Red, dashed vertical is the physical test mean and the dashed and dotted black line the CAE position.

Figure 43 display the heel X- and Z-coordinate variation from physical testing compared to the automatically positioned 50th percentile Hybrid III ATD. The X-coordinate was located close to the mean while the Z-coordinate was positioned approximately one standard deviation above the mean from physical testing.

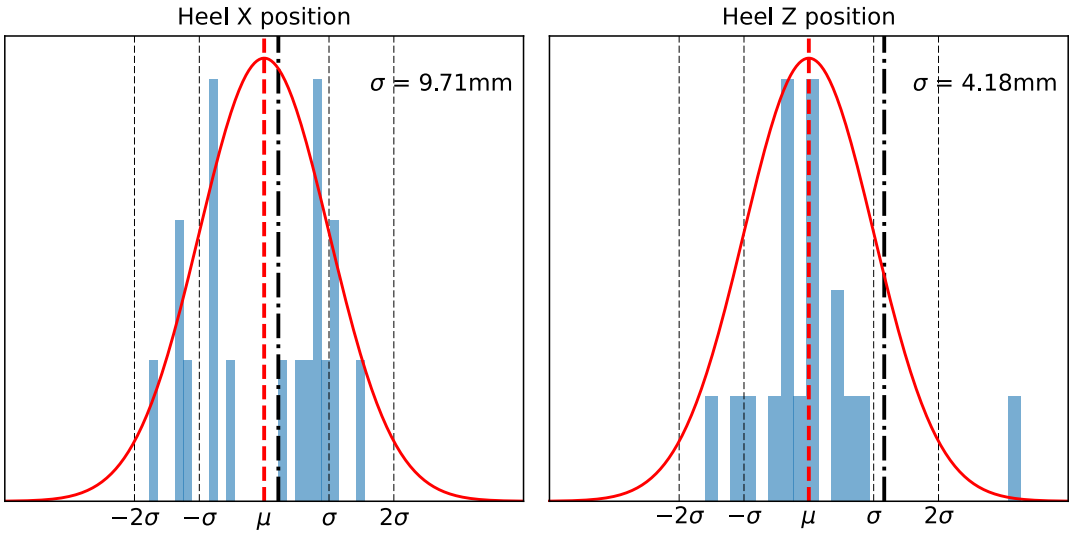

Figure 43: Heel X- and Z-coordinate from physical testing compared to CAE. Red, dashed vertical is the physical test mean and the dashed and dotted black line the CAE position.

In *Figure 44*, the heel positions of the physically positioned ATDs are compared with the automatically positioned ATD in CAE. The coordinates from the physical ATDs are displayed in black, and the automatically positioned ATD in red. As shown, the automatically positioned ATD is located above the cluster consisting of physical ATDs positions.

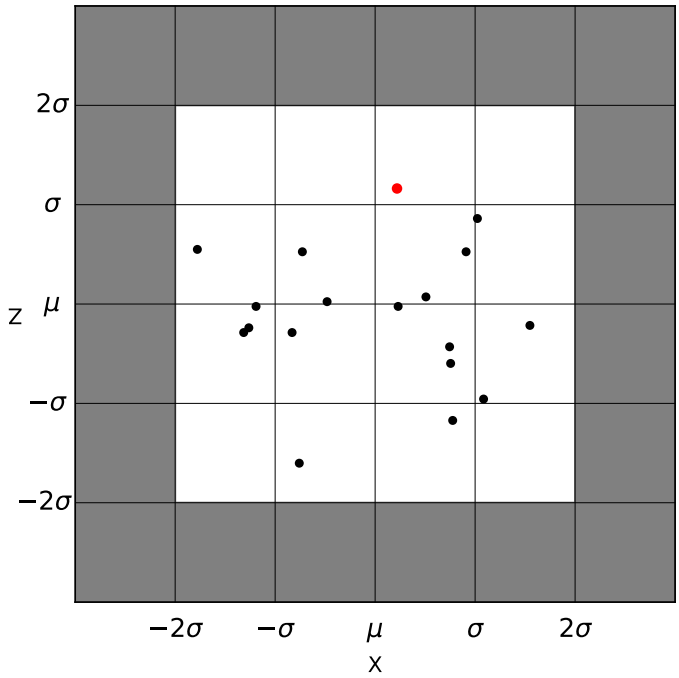

Figure 44: Scatter plot of heel positions from physical positioning, shown in black, compared to the automatically positioned ATD, shown in red.

4.2 Application studies: Injury Criteria variation

In this chapter the results from the injury criteria variation study are presented. A total of 31 simulations were executed. Seven simulations were conducted studying variations due to model decomposition using the mean H-point position from physical ATD positioning with varying amount of CPU cores. Furthermore, 25 different H-point positions, ranging from negative two standard deviations to positive two standard deviations in both X and Z direction, was simulated. All 31 simulations reached a normal termination and the injury criteria evaluated showed CVs ranging from 0,65% to 4,22%. The injury criteria values in this chapter have been normalized around the nominal H-point position, showing only the difference in injury criteria value measured. One standard deviation on the X-axis was 4.20 mm and 4.76 mm on the Z-axis in terms of H-point movement. Neck compression was excluded as small compressive forces was measured during the simulations.

4.2.1 Model decomposition

The injury criterion showed different sensitivity to variations in model decomposition, with CVs ranging from 0.65% to 4.22% in this simulation setup. The axial force through the right femur had the highest CV of 4.22% and a standard deviation of 0.08 kN. The left femur force was less sensitive to model decomposition, showing a CV of 2.52% and a standard deviation of 0.05 kN. Least sensitive was chest deflection showing a CV of 0.65% and a standard deviation of 0.12 mm. NIJ had a CV of 3.78% and a standard deviation 0.01 while its component neck tension showed a CV of 1.10% and a standard deviation of 0.01 kN. HIC_{15} had a CV of 3.28% and a standard deviation of 6.7%. Summary of the results can be found in *Table 2*.

Table 2: Summary of results from study on injury criteria variation due to model decomposition.

	CV	**Standard deviation**
$\boldsymbol{HIC_{15}}$	3.28%	6.7
$\boldsymbol{N_{ij}}$	3.78%	0.01
Neck tension	1.10%	0.01 kN
Chest deflection	0.65%	0.12 mm
Left femur force	2.52%	0.05 kN
Right femur force	4.22%	0.08 kN

Table 3 shows normalized HIC_{15} as result of change in CPU core count. Simulating using 160 CPU cores resulted in the highest HIC_{15} as all other CPU core counts resulted in lower values. The lowest recorded value deviated -21 point away from the nominal value using 160 CPU cores. The difference between the maximum and minimum value recorded was 21 points.

Table 3: Normalized HIC15 as result of changes in CPU core count.

HIC_{15}							
CPU	130	140	150	160	170	180	190
Diff	-21	-6	-14	0	-18	-9	-14

Min Max

Table 4 normalized N_{ij} as result of changing the CPU core count. The lowest recorded value deviated from the nominal value using 160 CPU cores with -0,01 points. The highest N_{ij} deviated 0,02 points from the nominal simulation. The difference between the highest and lowest recorded value was 0,03 points.

Table 4: Normalized NIJ as result of changes in CPU core count.

N_{ij}							
CPU	130	140	150	160	170	180	190
Diff	0,00	0,00	-0,01	0,00	0,00	0,02	0,01

Min Max

Table 5 shows normalized neck upper force as result of changes in CPU core count. The simulations using 150 and 190 CPU cores resulted in the highest neck tensions, deviating from the nominal simulation with 0,02 kN. The lowest value was recorded using 130 CPU cores and deviated from the nominal simulation with -0,01 kN. The difference between the highest and lowest force recorded was 0,03 kN

Table 5: Normalized neck upper force as result of changes in CPU core count.

NUF Z+ [kN]							
CPU	130	140	150	160	170	180	190
Diff	-0,01	0,00	0,02	0,00	0,01	0,01	0,02

Min Max

Table 6 shows normalized chest deflection as result of changes in CPU core count. The lowest values were recorded in the simulations using 170 and 190 CPU cores. The chest deflection for the simulation using 190 CPU cores was the lowest, deviating with -0,23 mm from the nominal chest deflection. The highest value deviated 0,17 mm from the nominal chest deflection and was recorded using 140 CPU cores. The difference between the highest and lowest deflections recorded was 0,4 mm.

Table 6: Normalized chest deflection as result of changes in CPU core count.

CD [mm]							
CPU	130	140	150	160	170	180	190
Diff	-0,14	0,17	-0,01	0,00	-0,20	-0,02	-0,23

Min Max

Table 7 shows normalized left femur force as result of changes in CPU core count. The highest left femur force was recorded using 190 CPU cores and deviated from the nominal simulation with 0.07 kN. The three lowest values of left femur force were recorded using 130, 170 and 180 CPU cores. Both the simulations using 170 and 180 CPU cores deviated from the nominal value with -0,06 kN. The difference between the highest and lowest left femur forces recorded was 0,13 kN.

Table 7: Normalized left femur force as result of changes in CPU core count.

FF Z- LEFT [kN]							
CPU	130	140	150	160	170	180	190
Diff	-0,05	0,02	0,01	0,00	-0,06	-0,06	0,07

Min Max

Table 8 shows normalized right femur force as result of changes in CPU core count. The highest values were recorded in the simulations using 170 and 180 CPU cores, deviating from the nominal simulation with 0,19 kN and 0,20 kN, respectively. The nominal simulation using 160 CPU cores recorded the lowest right femur forces. The difference between the highest and lowest right femur forces recorded was 0,20 kN.

Table 8: Normalized right femur force as result of changes in CPU core count.

FF Z- RIGHT [kN]							
CPU	130	140	150	160	170	180	190
Diff	0,06	0,05	0,03	0,00	0,19	0,20	0,02

Min Max

4.2.2 H-point movement

The differences in HIC_{15}, as a result of varying H-point positions can be seen in *Table 9*. The highest recorded value deviated 20 points away from the nominal H-point position while the lowest recorded value deviated -27 points from the nominal H-point position. A cluster of marginally higher HIC_{15} values can be found diagonally from sitting high forward to low rearward in the seat.

Table 9: Normalized HIC15 as result of H-point variation.

HIC_{15}					
	-2 σ_x	-1 σ_x	μ_x	1 σ_x	2 σ_x
2 σ_z	19	4	-18	-1	-14
1 σ_z	-7	11	-2	-27	-21
μ_z	-6	20	0	-23	-18
-1 σ_z	-10	9	-24	6	-4
-2 σ_z	-9	-7	-22	2	9

Min Max

N_{ij} variation by moving the H-point position seen in *Table 10* below. The highest score was 0,02 over the recorded nominal H-point position. The lowest recorded score was 0,02 points below the nominal value.

Table 10: Normalized N_{ij} as result of H-point variation.

N_{ij}					
	-2 σ_x	-1 σ_x	μ_x	1 σ_x	2 σ_x
2 σ_z	-0,01	0,01	-0,02	-0,01	0,01
1 σ_z	-0,02	-0,01	0,00	-0,01	-0,01
μ_z	0,00	0,00	0,00	-0,01	0,01
-1 σ_z	0,00	0,02	0,00	0,01	0,00
-2 σ_z	0,00	0,01	-0,01	0,01	0,01

Min Max

The highest value recorded for neck tension by moving the H-point deviated 0,16 kN from the nominal H-point position and was seated two standard deviations below the nominal H-point position. The lowest neck tension deviated -0,07 from the nominal position. *Table 11* shows the neck force as a result of moving the H-point.

Table 11: Normalized neck upper force as result of H-point variation.

NUF Z+ [kN]					
	-2 σ_x	-1 σ_x	μ_x	1 σ_x	2 σ_x
2	0,04	0,02	-0,01	0,01	0,00
1	-0,03	-0,07	0,01	0,07	0,06
μ_z	0,07	0,05	0,00	0,03	0,06
-1	0,06	0,09	0,09	0,01	0,06
-2	0,06	0,14	0,16	0,03	0,05

Min Max

The highest chest deflection measured, from moving the H-point position, deviated from the nominal with 2,32 mm while the smallest was -1,17 mm. The total spread of the dataset of approximately 3,5 mm. The chest deflection as a result of moving the H-point can be seen in *Table 12* below. A cluster of higher chest deflection values can be seen in high up, rearwards in the seat. Opposite, lower chest deflections was measured low down and forward in the seat.

Table 12: Normalized chest deflection as function of H-point variation.

CD [mm]					
	-2 σ_x	-1 σ_x	μ_x	1 σ_x	2 σ_x
2 σ_z	0,51	0,93	1,11	0,82	2,32
1 σ_z	0,21	0,03	-0,05	0,72	1,93
μ_z	-0,07	0,00	0,00	0,14	0,40
-1 σ_z	-0,61	-0,44	0,90	-0,60	-0,14
-2 σ_z	-1,17	-0,80	-0,31	-0,42	-0,50

Min Max

Furthermore, inspecting the difference in nose-to-belt distance, shown in *Table 13*, all belts crossed the chest above the initial position of the chest displacement transducer-lever connection to the slider. The H-point position with the highest chest deflection had belt routed closest to the initial position of the chest deflection transducer and the largest nose-to-belt distance. Similarly, the H-point position with the least amount of chest deflection had the belt routed furthest away from the chest displacement transducer measurement point.

Table 13: Normalized nose-to-belt distance.

Nose-to-Belt [mm]					
	$-2\ \sigma_x$	$-1\ \sigma_x$	μ_x	$1\ \sigma_x$	$2\ \sigma_x$
$2\ \sigma_z$	11,41	11,78	17,02	18,34	19,67
$1\ \sigma_z$	8,56	9,91	11,46	13,22	10,79
μ_z	4,05	4,98	0,00	8,52	10,42
$-1\ \sigma_z$	-1,13	1,30	0,04	7,78	5,23
$-2\ \sigma_z$	-7,68	-3,81	-2,16	-0,67	1,23

Min Max

The highest relative femur force in the left leg was measured at 0,73 kN above the nominal measurement. The lowest femur force was recorded at -0,46 kN relative the nominal H-point position. The left femur force relative the nominal H-point position is shown in *Table 14* below.

Table 14: Normalized left femur force as function of H-point variation.

FF Z- LEFT [kN]					
	$-2\ \sigma_x$	$-1\ \sigma_x$	μ_x	$1\ \sigma_x$	$2\ \sigma_x$
$2\ \sigma_z$	0,73	0,33	0,09	0,10	-0,01
$1\ \sigma_z$	0,33	0,41	0,04	-0,15	-0,13
μ_z	0,20	-0,13	0,00	-0,16	-0,04
$-1\ \sigma_z$	0,02	0,17	-0,10	-0,44	-0,46
$-2\ \sigma_z$	0,12	-0,09	-0,12	-0,15	-0,34

Min Max

Values in the range of -0,29 to 0,55 kN of right femur force relative the nominal H-point position was recorded, as seen in *Table 15* below. For both femurs, the forces measured increased forwards and upwards in the seat. The lowest forces of both datasets could be found at the rearmost bottom H-point position.

Table 15: Normalized right femur force as function of H-point variation.

FF Z- RIGHT [kN]					
	$-2\ \sigma_x$	$-1\ \sigma_x$	μ_x	$1\ \sigma_x$	$2\ \sigma_x$
$2\ \sigma_z$	0,55	0,59	0,18	0,38	0,19
$1\ \sigma_z$	0,31	0,30	0,28	0,22	0,02
μ_z	0,52	0,22	0,00	0,03	-0,12
$-1\ \sigma_z$	0,41	0,04	0,12	-0,09	0,09
$-2\ \sigma_z$	-0,06	0,08	0,13	-0,20	-0,29

Min Max

5 Discussion

This thesis assessed the possibility of automating the time-consuming task of ATD positioning as well as assessing injury criteria variations in simulations. The injury criteria variation application studies consisted of two parts, one assessing the reproducibility of the 50th percentile male Hybrid III ATD and one assessing injury criteria variations due to H-point positioning. H-point positioning was found to vary in the physical test data studied. The physical H-point positioning data was used for validation of the automated positioning method as well as for the study about injury criteria variations due to H-point positioning.

5.1 Physical ATD positioning data

ATD positioning measurements from physical crash tests were used for validation of the automated positioning method and furthermore, for assessing injury criteria dependency on H-point positioning. A total of six different ATD coordinates was considered, and ten out of twelve measurements showed to be normally distributed at the five percent significance level, possibly caused by outliers in the positioning data sets. Additionally, in the collected data points for H-point, knee, and heel X-coordinates, in physical testing, performed for the car model, according to the US NCAP full frontal rigid barrier 35 mph protocol, two clusters of X-coordinates were observed. Although, the cluster did not cause these data sets to not be normally distributed.

Possibly, the clusters formed by the physical positioning data was an effect of the seat slider being positioned slightly different in between physical tests. In seats with manual seat adjustment utilizing stepped rails, this could be an effect of needing to choose between steps in the rails. Although, for seats with powered seating adjustment, they can be adjusted linearly, thus the seat slider can be positioned perfectly. It may also be contributed to interpretation of protocols and how the seat slider was adjusted and measured.

If there were variations in seat slider positioning, it would cause the R-point to be located differently in the car coordinates system and thus, the H-point when it was positioned in the seat. Positioning variations in ATD coordinates located in the upstream of a limb will consequentially cause errors for the coordinates downstream. Therefore, the clusters seen in H-point positioning will be reflected in positioning of both knee and heel positioning.

5.2 Automated positioning method

In physical ATDs, reproducibility in repeated tests have been studied previously. Due to manufacturing tolerances, ATD wear, positioning variance and other environmental test circumstances, repeated tests have variations. When compared to CAE, some of variations found in physical ATDs are not applicable, but other variations are introduced. Manufacturing tolerances is replaced by accuracy of modelling and environmental test circumstances by solver settings, computer system and number of CPU cores. Furthermore, ATD positioning performed by hand in CAE, according to protocols formulated for physical ATD positioning, might introduce variations due to human factors.

Automated ATD positioning in CAE has shown to be possible, reducing the time consumption of the procedure drastically. The automated positioning method can position ATDs within one standard deviation of the measurements found in physical tests for head CoG, nose, shoulders, and feet. By removing the human factor, repeatability of the positioning process increases. The method will, assuming providing the same ATD and vehicle model as well as applying the same settings, position the ATD the same every time. The automated positioning method, in its existing form, require some tuning of settings to get an acceptable ATD position for new car environments. To account for the issues that can occur if the implementation was not tuned properly, the implementation of the automated positioning method will pause, allowing the user to amend the ATD position before continuing creating the ATD pre-simulation. In some occurrences, the implementation got stuck or crashed which implies that there is room for reliability improvements. A finding was that the implementation of the automated positioning method struggles with the same environments that human operators also would consider more difficult, e.g., positioning the 95th percentile Hybrid III ATD in a small second row seating position or when the fifth percentile Hybrid III ATD cannot reach the floor.

In addition, related to the car environment for certain ATD models and protocols; protocol exceptions were not implemented in the automated positioning method as they are apparent challenges in physical ATD positioning as well. One of the problems that could occur for the fifth percentile Hybrid III, was if the seat cushion was too deep or the H-point positioned too far back; the calves then intersected the seat cushion before feet contacted the floor when lowering the lower leg. For the 95th percentile Hybrid III, the chest and shoulders may be wider than the backrest of the front seats, resulting in misplacement of the upper arm as it does not come in contact with the backrest and consequentially misplacing the hands.

During development of the automated positioning method, only the Hybrid III adult ATDs have been considered. Although, if the ATD model prerequisites and the joint structures of other ATDs are similar, more ATD models should be possible to implement. As for now, the implementation of the automated positioning method was developed to work with the existing workflow of the car manufacturer. If a fully general implementation of the automated positioning script can be developed remain unexplored. To further improve the implementation of the automated positioning method using ANSA, new API functions would be of benefit. For positioning the thighs, they should be positioned intersecting the seat cushion to compress the seat cushion foam during the initial phase of the simulation. With the current method using intersections to position limbs the rotation of the thighs would stop as soon as they come into contact with the seat cushion. To solve the issue, it was allowed for the thighs to rotate a few extra degrees. Although, depending on the H-point position and seat cushion geometry the number of degrees from the initial thigh intersection needs to be tuned to achieve the correct amount of thigh intersection. An incorrect estimation of this parameter will cause consequential faults as misplacing legs and feet or programming error executing the implementation of the automated positioning method. To have such a sensitive user-changeable parameter is not favourable. A suggestion is to, for instance, develop functions that support measuring intersection distance. It could significantly increase reliability and accuracy of the implementation of the automated positioning method. As well as decrease the amount of workload, trial, and error, of the operator.

The automated positioning method was shown to be able to position the Hybrid III 50th percentile male in the driver seat, within the measured spread of physical positioning for all the measured locations on the ATD except knee-position X-coordinate. The knee-position was dependent on a number of factors such as thigh intersection with seat cushion as well as knee Y-position which has not been taken into consideration in the validation. Although, when reviewing Y-position of the knee, a posteriori, in CAE, it was concluded that the knees positioned by the automated positioning method was located further apart than the knees of the ATDs positioned in physical testing. Differences in interpretation of the protocol and changes of internal ATD positioning guidelines could also be the reason of the differentiation. Furthermore, there was uncertainties regarding measurement location for knee-coordinates in physical ATD positioning and how it should be replicated in CAE.

Positioning ATDs in CAE has some limitations that need to be taken into consideration when comparing the performance of the automated positioning method to physical ATD positioning measurements. A quite simple example is, in physical positioning of ATDs, positioning the feet resting on the carpet. In CAE positioning ATDs in contact with the car environment is a challenge, as no parts that are not intended to be included in the pre-simulation of the ATD can intersect the ATD model. If so, intersections in the simulation can cause numerical issues once running the full simulation. Including more parts than necessary in the ATD pre-simulation can also be problematic, as it, among more, increases the simulation time and work associated with pre-simulation setup. This was the case regarding heel Z-coordinate location being located above the mean heel Z-coordinate from physical testing.

5.3 Application studies: Injury criteria variation

The first application study explored numerical reproducibility of injury criteria using the Hybrid III 50th percentile male ATD in one frontal crash simulations. Numerical reproducibility was in this study defined as replication of simulation result given varying simulation settings. To study this, several simulations were conducted on an HPC, using the same FE models but executed using varying amount of CPU cores. Distributing the numerical workload of complex FE simulation over several CPU cores is common behaviour in CAE to shorten the calculation time, as modern FE crash simulations is far too large to be run on a single core time efficiently. Although, this speed-oriented approach is known to cause imperfect reproducibility. Varying the number of CPU cores will result in a different model decomposition. The different model decomposition will accordingly cause variation in CPU communication, numerical round-off which can be seen as different amplitude of global injury criteria.

As for the second application study, the global injury criteria were reviewed when moving the H-point. This part was based upon the H-point variations found in the statistical analysis of physical tests done to validate the automated positioning method and estimation of H-point positioning for CAE. A total of 25 different H-point positions was simulated covering 95% of the physical tests performed as well as the CAE H-point estimation for that specific car model. The ATDs were positioned using the implementation of the automated positioning method and belts routed individually by hand for all ATDs. Even though these simulations were executed using the same number of CPU cores, the slight changes in ATD positioning gave variations in injury criteria values. This effect, evaluated in the first part of the study, was considered as noise throughout the second part of the study.

5.3.1 Injury criteria variations due to model decomposition

In this study, the Hybrid III 50th percentile male exhibited a numerical reproducibility CV ranging from 0.65% to 4,22%, hence high numerical reproducibility across all the evaluated injury criterion. In perspective, (NHTSA, 2013) classifies a CV of less then 5% as excellent in regards to physical ATD reproducability. In line with the findings of (Östh et al., 2021), chest deflection was the most reproducible with a CV of 0.65%. HIC produced a CV of 3,28% which was less then the physical Hybrid III 50th percentile male showed in the study by (Foster, 1977). In summary, model decomposition showed to produce disturbances to reproducability on approximately the same or lower levels then found in physical testing.

5.3.2 Injury criterion variations due to H-point movement

The difference from highest to lowest measured chest deflection was 3.5 mm. The lowest deflection for H-point positions far forward and low down in the seat as the highest chest deflections were measured for H-point positions high up and far back in the seat. This can be referred to the shoulder belt and the chest deflection sensor location as chest deflection is well documented to be sensitive to load location for the Hybrid III ATDs (Haight et al., 2013). Upon reviewing the shoulder belt location, it was concluded, due to location of the fixed D-ring, that the lowest measured chest deflections also had the largest mismatch between belt and sensor location. Due to the well documented issue measuring chest deflection, new chest deflection measurement systems have been developed, as the IR-TRACC system. Some protocols, where the Hybrid III ATDs is used, incorporate a pressure vest to further investigate belt and ATD interaction (Insurance Institute for Highway Safety, 2022).

For the femur forces, sitting high and forward in the seat led to higher forces due to interactions with the knee-airbag in simulations. Sitting far back and low in the seat, resulted in lower contact forces as the occupant's pelvis forward movement, and thus femur forward movement, was restrained more by the lap-belt.

As for neck extension, the lowest seating positions resulted in higher neck tension forces in the simulation, which might be caused by the ATDs head rotating encountering the airbag, turning its cheek towards the airbag. HIC and N_{ij} showed to be unsensitive to H-point movement in this study, as both showed variations in-line with the variations measured during model decomposition.

When positioning ATDs, H-point position is of utmost importance as the pelvis is highest in the limb-tree hierarchy. Variations in H-point position will cause positioning of other limbs to vary. The H-point position had considerable effect on some of the global injury criteria evaluated. Variations in H-point positioning also showed to affect injury criteria more than model decomposition although, only small changes in H-point position were tested. In addition, the H-point positions tested were retrieved statistically from physical crash tests. Therefore, the study highlighted the importance of achieving the correct H-point positioning, in CAE as well as in physical tests. The result implies that by implementing procedures to mitigate variations in ATD positioning, reproducibility can be improved.

6 Conclusion

An automated ATD positioning method was developed and demonstrated to be viable for the three sizes of adult Hybrid III anthropomorphic test devices in an CAE environment. The implementation of the automated positioning method could position ATD models in a variety of car models within five to ten minutes, thereby reducing the manual labour associated with the ATD positioning procedure.

In US NCAP full frontal rigid barrier 35 mph and mid-size SUV evaluated, reproducibility Coefficient of Variation for the Hybrid III 50th percentile male varied between 0.65% to 4.22% for different injury criteria. The right femur force was the most sensitive injury criterion regarding model decomposition, while chest deflection showed to be the least sensitive, as they had the highest and lowest CVs in this simulation, respectively.

In the application study, evaluating injury criteria for different H-point positions, some responses showed to be sensitive to H-point positioning. Especially sensitive was chest deflection, showing total variations in chest deflections of up to 3.5 mm, and femur force which varied up to one kN. Injury criteria were generally more sensitive to the relative narrow spread of H-point positions tested than to model decomposition. This stresses the importance of correctly positioning ATDs in physical crash tests as for estimating the correct R-point coordinates in CAE while implying a need to mitigate variations in ATD positioning.

7 Future Work

This thesis developed an automated ATD positioning method and demonstrated it using the adult size Hybrid III dummies. However, there is more work that can be done to improve accuracy, reliability, and functionality of the automated positioning method. One of the most pressing matters is to automatize the maximum allowed thigh intersection. Automatic recognition of how much thigh intersection is appropriate will improve the reliability for positioning in seat positions, ATD H-point positions as well as pelvis angles that do not follow any prescribed protocol. Furthermore, adding support for protocol exceptions would lower the number of corrections the user may have to do manually, especially regarding fifth percentile Hybrid III female in driver seat.

For now, the automated positioning has been developed for only the Hybrid III adult ATDs, using a limited set of car environments. Although, adapting the automated positioning method for other ATDs and load cases are highly relevant. Furthermore, the THOR 50M ATD is gaining in popularity, replacing the Hybrid III 50th percentile male in frontal collision tests. As the interest of virtual verification of requirements using the Human Body Model (HBM) grow, an automated positioning method for HMBs should be investigated.

To fully automate the setup of pre-simulation, an automated method for belt-routing should be developed as this task also is time consuming and meticulous without contributing with additional value to the analysis. Furthermore, the process of positioning the seat model could be automated as well as assembling the car environment file with its included components.

In regards to saving time, the limb-positioning functions within the implementation that are not dependent on each other, e.g., left, and right arm, could be run in parallel to shorten execution time. In the time of writing, this is not supported by the simulation pre-processor used during development.

8 References

49 CFR 571.271 Revised as of Apr. 9, 2004.

49 CFR 572.33 Revised as of Apr. 9, 2004.

49 CFR 572.36 Revised as of Apr. 9, 2004.

Altair (n.d.). *FE Dummy Models by Humanetics*. Retrieved *June* 20, 2023, from https://altair.com/fe-dummy-models.

Amirouche, F. M. L. (2006). *Fundamentals of Multibody Dynamics* (1st ed.). Birkhäuser Boston, MA. https://doi.org/10.1007/b137682.

Belytschko, T., Liu, W. K., Moran, B., & Elkhodary, K. I. (2014). *Nonlinear Finite Elements for Continua and Structures* (2nd ed.). John Wiley & Sons. https://doi.org/10.1007/b137682.

CARHS. (2022, December 23). *Protection Criteria in Frontal and Side Impact (U.S. NCAP)*. SAFETYWISSEN. Retrieved May 12, 2023, from https://www.safetywissen.com/object/B04/B04.sxl738529vhuhy89ru782353xs2dxn63808901553/safetywissen?prev=%2Frequirement%2FW02.ypy7375519m704t6wy9391579y09mr63724359157%2F.

CARHS. (n.d.). *Requirements*. SAFETYWISSEN. Retrieved May 25, 2023, from https://www.safetywissen.com/requirement/W02.7op734840t7ab31mhk975320tmcj0q63490164920/.

Díaz, J., & Costas, M. (2020). *Encyclopedia of Continuum Mechanics* (pp. 469-486). Springer Berlin, Heidelberg. https://doi.org/10.1007/978-3-662-53605-6.

Diethelm, K. (2012). The limits of reproducibility in numerical simulation. Computing in Science & Engineering, 14(1), 64–72. doi:10.1109/mcse.2011.21.

European Commission. (n.d.). *Consumer information*. Mobility & Transport - Road Safety. Retrieved May 2, 2023, from https://road-safety.transport.ec.europa.eu/eu-road-safety-policy/priorities/safe-vehicles/archive/consumer-information_en.

Foster, J., Kortge, J., and Wolanin, M., (1977). "Hybrid III-A Biomechanically-Based Crash Test Dummy," SAE Technical Paper 770938, https://doi.org/10.4271/770938.

Germanetti, F., Fiumarella, D., Belingardi, G., & Scattina, A. (2022). Injury Criteria for Vehicle Safety Assessment: A Review with a Focus Using Human Body Models. Vehicles, 4(4), 1080–1095. https://doi.org/10.3390/vehicles4040057.

Gillis, A. S., & Bigelow, S. J. (2022, July). Message passing interface (MPI). TechTarget. Retrieved March 13, 2023, from https://www.techtarget.com/searchenterprisedesktop/definition/message-passing-interface-MPI.

Haight, S., Samaha, R. R., & Biss, D. (2013). Analysis of seat belt positioning in recent NCAP crash tests. SAE International Journal of Transportation Safety, 1(1), 16–24. doi:10.4271/2013-01-0460.

Harish, A. (2020, November 29). Implicit vs Explicit Finite Element Method (FEM): What Is the Difference? SIMSCALE. Retrieved February 24, 2023, from https://www.simscale.com/blog/implicit-vs-explicit-fem/.

Hellqvist, T., & Rattfelt, T. (2017). Sensitivity of H-point Parameters in CAE Prediction of Automotive Seats. Gothenburg: Chalmers University of Technology.

Hershman, L. L. (2001). THE U.S. NEW CAR ASSESSMENT PROGRAM (NCAP): PAST, PRESENT AND FUTURE. PROCEEDINGS OF 17TH INTERNATIONAL TECHNICAL CONFERENCE ON THE ENHANCED SAFETY OF VEHICLES. Amsterdam, Netherlands: National Highway Traffic Safety Administration.

Humanetics Innovative Solutions, Inc. (n.d.). Hybrid III 50th Male. HUMANETICS. Retrieved March 20, 2023, from https://www.humaneticsgroup.com/products/anthropomorphic-test-devices/frontal-impact/hybrid-iii-50th-male/hybrid-iii-50th-male.

Humanetics Innovative Solutions, Inc. (n.d.). *Hybrid III 50th Male FE*. HUMANTECIS. Retrieved June 20, 2023, from https://www.humaneticsgroup.com/products/virtual-models/frontal-impact-atd-virtual-models/hybrid-iii-50th-male-fe/harmonized-0.

Humanetics Innovative Solutions, Inc. (2019). Harmonized Hybrid III 50M Dummy LS-DYNA.

Insurance Institute for Highway Safety. (2022). Moderate Overlap Frontal Crashworthiness Evaluation 2.0: Version 1. Ruckersville.

Insurance Institute for Highway Safety (n.d.). *About our tests*. IIHS-HLDI. Retrieved May 10, 2023, from https://www.iihs.org/ratings/about-our-tests.

Jakobsson, L., Lindman, M., Axelson, A., Lokensgard, B., Petersson, M., Svanberg, B., & Kovaceva, J. (2014). Addressing run off road safety. SAE International Journal of Passenger Cars - Mechanical Systems, 7(1), 132–144. doi:10.4271/2014-01-0554.

Jakobsson, L., Björklund, M., & Westerlund, A. (2016). Thoracolumbar Spine Injuries in Car Crashes. IRCOBI Conference (pp. 101 - 112). Malaga, Spain: International Research Council on the Biomechanics of Injury.

Johnson, D., Koya, B., & Gayzik, F. S. (2020). Comparison of neck injury criteria values across human body models of varying complexity. Frontiers in Bioengineering and Biotechnology, 8, 985. doi:10.3389/fbioe.2020.00985.

Keegan, M. C. (2017, April 20). *The History of Car Safety Ratings*. NAPA BLOG. Retrieved May 16, 2023, from https://knowhow.napaonline.com/history-car-safety-ratings/.

Kim, T., Funk, J. R., Bollapragada, V., Ye, X., & Crandall, J. (2017). Evaluation of biofidelity and repeatability of THOR-Lx metric under axial impact loading. International Journal of Precision Engineering and Manufacturing, 18(7), 1027–1034. doi:10.1007/s12541-017-0121-5.

Kondo, K. (2012). Fujitsu's Activities in Improving Performance of LS-DYNA Nonlinear Finite Element Analysis. Fujitsu Scientific and Technical Journal 48(3), 375–383.

LSTC. (2007). LS_DYNA Keyword User's Manual: Volume 1.

Malato, G. (n.d.). *A practical introduction to the Shapiro-Wilk test for normality*. Towards Data Science. Retrieved May 24, 2023, from https://towardsdatascience.com/a-practical-introduction-to-the-shapiro-wilk-test-for-normality-5675e52cee8f.

NHTSA. (2013). 49 CFR Part 572. Anthropomorphic Test Devices: Q3s 3-Year-Old Child Side Impact Test Dummy. Federal Register.

NHTSA (n.d.). Timeline. Retrieved May 16, 2023, from https://one.nhtsa.gov/nhtsa/timeline/index.html.

Nice, K. (n.d.). *How Crash Testing Works*. Howstuffworks. Retrieved May 15, 2023, from https://auto.howstuffworks.com/car-driving-safety/accidents-hazardous-conditions/crash-test.htm.

Östh, J., Pipkorn, B., Forsberg, J., & Iraeus, J. (2021). Numerical Reproducibility of Human Body Model Crash Simulations. International Research Council on Biomechanics of Injury, (pp. 431-443). Online.

Rouhana, S. W. (1998). A high-speed sensor for measuring chest deflection in crash test dummies. In Proceedings: International Technical Conference on the Enhanced Safety of Vehicles (Vol. 1998, pp. 2017-2045). National Highway Traffic Safety Administration.

Schmitt, K.-U. (2009). Trauma Biomechanics: Accidental injury in traffic and sports. 3rd Edition. Zurich: Springer.

Skotny, Ł. (2019, February 3). *How Accurate is Finite Element Analysis?* Enterfea. Retrieved June 15, 2023, from https://enterfea.com/how-accurate-is-finite-element-analysis/.

Toney-Butler, T. J., & Varacallo, M. (2022, August 29). *Motor Vehicle Collisions*. National Library of Medicine. Retrieved March 19, 2023, from https://www.ncbi.nlm.nih.gov/books/NBK441955/.

UNECE. (2021). UN Regulation No. 17. United Nations.

United Nations (n.d.). *Make cities and human settlements inclusive, safe, resilient and sustainable*. United Nations Department of Economic and Social Affairs Sustainable Development. Retrieved May 2, 2023, from https://sdgs.un.org/goals/goal11.

World Health Organization (2022, June 20). *Road traffic injuries*. Retrieved January 18, 2023, from https://www.who.int/news-room/fact-sheets/detail/road-traffic-injuries

DEPARTMENT OF MECHANICS AND
MARITIME SCIENCES
CHALMERS UNIVERSITY OF TECHNOLOGY
Gothenburg, Sweden 2023
www.chalmers.se

CHALMERS
UNIVERSITY OF TECHNOLOGY